Flow past cylindrical obstacles on a beta-plane

By MICHAEL A. PAGE[1] AND E. R. JOHNSON[2]

[1] Department of Mathematics, Monash University, Clayton, Victoria 3168, Australia
[2] Department of Mathematics, University College, London WC1E 6BT, UK

The flow past a cylindrical obstacle in an enclosed channel is examined when the entire configuration is rotating rapidly about an axis which is aligned with that of the obstacle. When viewed from a frame of reference which is rotating with the channel, Coriolis forces dominate and act to constrain the motion to be two-dimensional. The channel is considered to have depth varying linearly across its width, producing effects equivalent to the so-called β-plane approximation and permitting waves to travel away from the obstacle, both upstream and downstream. For the eastward flow considered in this paper, this leads to the formation of a lee-wavetrain downstream of the obstacle and, under some conditions, a region of retarded, or 'blocked', flow upstream of the obstacle. The flow regime studied is essentially inviscid, although one form of frictional effect on the flow, introduced through the Ekman layers, is included. The properties of this system are examined numerically and compared with the theoretical predictions from other studies, which are applicable in asymptotic limits of the parameters. In particular, the relevance of 'Long's model' solutions is considered.

1. Introduction

The study of flows observed from a rotating frame of reference is clearly of relevance to large-scale motion in the oceans and atmosphere, where Coriolis forces due to the earth's rotation play a significant role in the dynamics. Although both the ocean and atmosphere are density-stratified, much can be gained from studying the motion of homogeneous fluid under similar circumstances. The next step in the study of large-scale geophysical flows is to include effects due to the latitudinal variation of apparent rotation rate, and this is usually modelled by the so-called β-plane approximation which represents the variation linearly in mid-latitudes. The resulting spatial gradient of Coriolis force permits a form of wave motion which travels horizontally within the system; these waves known as Rossby waves, are dispersive and have the property that the longitudinal component of the phase velocity is always directed westwards. Since the group velocity can take any direction, some care is required on 'open' boundaries of the flow domain.

In this paper several important features of eastward β-plane flows are examined by considering the relatively simple model of a uniform flow past a cylindrical obstacle. The problem is studied over the complete parameter range in which inertial, β-plane and Ekman-suction effects are important, the last of which introduces a dissipative mechanism through friction in the Ekman layers on the top and bottom boundaries. The properties of rotating flows, under appropriate conditions, ensure that the fluid motion is dominantly two-dimensional and depth-independent, and this leads to significant simplifications of the analysis. The flow can then be described in terms of two dynamical parameters and the non-dimensional channel width, with

the effects of the other geometrical parameters generally of less importance. The resulting equations are also accessible to analysis in various asymptotic limits of the dynamical parameters and the results of this analysis are compared with the numerical solutions, where appropriate. In particular, the magnitude and extent of the disturbance caused by the obstacle is well described by the asymptotic theory.

Most of the properties of this configuration are independent of the particular shape of the obstacle introduced into the flow and so in this study a symmetric aerofoil, with a uniform cross-section over the depth of the fluid, has been chosen (for reasons which will be detailed later in this introduction). As is common in laboratory experiments, the β-plane effects will be modelled by a linear variation in depth of the channel across its width. This can be shown to be equivalent, analytically, to a linear variation in rotation rate across the channel (Greenspan 1970) and therefore flows in the study are equivalent to zonal flows in the oceans and atmosphere. The channel is also considered to have finite width and for computational reasons, outlined later, the channel in this study will be slightly wider near the obstacle than at the inflow and outflow regions. In the laboratory experiments of Boyer & Davies (1982) the channel has uniform width and the obstacle is a circular cylinder but similar effects can be expected (and are observed) in the configuration used here. The extensions to an infinite-width channel are feasible in principle, but a continuous set of allowable wave-modes must be accounted for.

As mentioned above, the β-effect allows Rossby waves to propagate within the system and these are apparent in the evolution of the flow past an obstacle. The oncoming stream tends to advect some of these downstream but there will always be some waves with a sufficiently large group velocity to propagate upstream of the obstacle. Thus, when the flow becomes steady (as it usually will after a sufficient time) the only waves remaining are the stationary waves with their phase speed equal to the local flow speed. In eastward flows these can form a 'lee-wavetrain' behind the obstacle, like that shown for internal waves in a stratified flow by Miles & Huppert (1968), but they can also significantly modify the oncoming uniform stream, in an extreme case forming a 'blocked' region upstream such as that illustrated in Foster (1985). The latter effect is similar to that described for a stratified fluid by Baines (1977) and, in the absence of dissipation, it can have a profound influence on the upstream boundary conditions and can limit the applicability of such 'Long's model' solutions as those in Miles & Huppert (1968). Although the effects of Ekman suction can be expected to modify these general properties, it will be seen from both the analytical and the numerical results presented in this paper that the features remain broadly appropriate in the presence of this form of dissipation. There are, however, some significant differences between the analysis and the numerical solutions, such as the 'resonant' effect in Long's model for a finite-width channel and (more generally) the formation of closed-streamline regions, and these are explained here in terms of the effects of stationary upstream waves. In contrast, neither upstream effects nor lee-wave wakes are present in westward flows past an obstacle (Johnson & Page 1990).

Another factor that should be taken into account, especially when comparing the analytical and numerical results with those obtained experimentally, is that the viscous boundary layers which are neglected in the analysis of this paper can separate from the obstacles and significantly distort the flow. This flow separation is similar to that seen in non-rotating flows at high Reynolds number, and it has been studied extensively in uniformly rotating, or f-plane, flows where β effects are neglected. In that situation it is found that once inertial effects begin to dominate

Ekman-dissipation, the $E^{\frac{1}{4}}$ layers on the obstacle can separate and enclose a finite region of stagnant fluid (Page 1987). With a β-plane approximation included the same situation arises, but the critical ratio of inertia to dissipation depends on the relative magnitude of the β effect, rather as it depended on the height of the topography in Page (1982). The effects of $E^{\frac{1}{4}}$-layer separation are not included explicitly in this study, but the criterion for separation is examined to determine whether they may be important. For bodies with a bluff trailing-edge, such as the circular cylinder, it is clear from previous studies (including Matsuura & Yamagata 1986) that separation occurs over most of the parameter regime considered in this paper, distorting the effective shape of the obstacle. To model the effect of this, the obstacle used in this study was chosen to have a cross-section in the form of a Joukowski aerofoil, of a similar shape to the separated flow for a large class of bluff obstacles (Page 1988).

Section 2 derives the governing equations showing that in the limit of vanishingly small viscosity the flow can be characterized by two parameters α and λ, measuring the strength relative to Ekman suction of, respectively, the β effect and advection. Sections 3–8 discuss briefly various asymptotic limits of these equations. Section 3 presents the limit of slow flow $\lambda \ll 1$ in which the governing equation becomes linear. It is shown that if also $\alpha \gg 1$ then any obstacle affects the flow far upstream. In §4 the same limit is considered with $\bar{\lambda} = \alpha\lambda$ fixed, which was introduced by Foster (1985) to discuss the first effects of nonlinearity on flow dominated by the linear balance between the β effect and Ekman suction. Section 5 then considers the general properties of flows with $\alpha \gg 1$, for which the β effect is dominant, while §6 discusses the inviscid limit $\lambda \to \infty$, $\alpha \to \infty$ with $\kappa = (\alpha/\lambda)^{\frac{1}{2}}$ fixed. In this regime the potential vorticity is conserved to leading order, giving 'Long's model' solutions equivalent to those derived for a stratified fluid by Miles & Huppert (1968). The limit $\lambda \gg 1$ and α is arbitrary is considered in §7, in which case Ekman suction only affects the flow over distances of $O(\lambda)$ from the obstacle. Finally, the case of weak β effect, $\alpha \ll 1$, is examined in §8 for arbitrary λ by expanding about the irrotational solution which is appropriate when $\alpha = 0$.

In §9 the numerical method used to solve the equations for arbitrary α and λ is presented and in §10 the results of these numerical integrations are discussed in relation to the various asymptotic solutions described in §§3–8. Section 11 discusses the conditions under which $E^{\frac{1}{4}}$ layers on the obstacle can separate and the types of flow pattern expected in that case. Finally, the overall conclusions are briefly summarized by §12.

2. Governing equations

This paper examines the motion of a homogeneous fluid of density ρ^* and constant kinematic viscosity ν^* which is contained in an infinitely long channel of finite depth d^*, rotating at constant angular velocity Ω^*. Relative to a frame of reference rotating with the channel, a uniform flow of speed U^* is introduced along the channel within which a cylindrical obstacle, of scale width l^*, is placed with its axis aligned vertically (i.e. parallel to the rotation axis). The base of the container is inclined by a small angle β from the horizontal, so that it slopes in the direction perpendicular to the introduced flow. This configuration is essentially the same as that considered by Foster (1985), Page & Johnson (1986), Matsuura & Yamagata (1986) and used in the experiments performed by Boyer & Davies (1982). It also parallels similar work on flows in an enclosed container by Pedlosky & Greenspan (1967), Beardsley (1969,

1973) and more recently by Hide & Hocking (1979). In fact, the derivation of the equations in this section follows the treatment in Hide & Hocking (1979). The particular case $\beta = 0$, often referred to as the f-plane flow, has also been examined extensively, most recently by Page (1987).

Based on the dimensional quantities described above, four non-dimensional parameters can be introduced

$$Ro = \frac{U^*}{\Omega^* l^*}, \quad E = \frac{\nu^*}{\Omega^* d^{*2}}, \quad \tan \beta, \quad d = \frac{d^*}{l^*}, \tag{2.1}$$

referred to here as the Rossby number, Ekman number, bottom slope and scaled depth, respectively. These form the basic set of governing parameters for the flow to be described in this paper, as can be demonstrated by non-dimensionalizing velocities in the flow with respect to U^*, lengths with respect to l^* and time with respect to $(\Omega^*)^{-1}$. The full governing equations for a fluid in this configuration are then

$$\frac{\partial \boldsymbol{u}}{\partial t} + Ro(\boldsymbol{u} \cdot \boldsymbol{\nabla}) \boldsymbol{u} + 2(\boldsymbol{k} \times \boldsymbol{u}) = -\boldsymbol{\nabla}P + E\nabla^2 \boldsymbol{u}, \tag{2.2}$$

$$\boldsymbol{\nabla} \cdot \boldsymbol{u} = 0, \tag{2.3}$$

where $\boldsymbol{k}$ is the unit vector in the z-direction and P is the reduced pressure (with the centrifugal contribution removed and scaled by $\rho^* U^* \Omega^* l^*$). For convenience, the horizontal axes are chosen so that x is aligned with the uniform flow at infinity and the bottom slope is in the y-direction.

The particular case of interest in this paper is where the Ekman number E tends to zero and both the Rossby number Ro and the bottom slope $\tan \beta$ are $O(E^{\frac{1}{4}})$, with d being an $O(1)$ quantity with respect to $E^{\frac{1}{2}}$. Under these conditions the steady flow is governed predominantly by the geostrophic balance

$$2(\boldsymbol{k} \times \boldsymbol{u}) \approx -\boldsymbol{\nabla}P, \tag{2.4}$$

which, in turn, implies that the basic flow is both two-dimensional and depth-independent. Details are standard, and can be found, for example, in Greenspan (1968) or Moore (1978). Further, if it is assumed that the flow varies on a relatively slow timescale of $O(E^{\frac{1}{4}})$ (which is acceptable once the original spin-up process has been completed) it can be shown that the vertical component of the vorticity

$$\zeta = \frac{\partial v}{\partial x} - \frac{\partial u}{\partial y}, \tag{2.5}$$

satisfies $$\frac{\partial \zeta}{\partial t} + Ro\left(u\frac{\partial \zeta}{\partial x} + v\frac{\partial \zeta}{\partial y}\right) = (2 + Ro\zeta)\frac{\partial w}{\partial z}, \tag{2.6}$$

where $\partial w/\partial z$ in this equation is of order $E^{\frac{1}{4}}$ and is induced solely by the Ekman layers near both $z = y \tan \beta$ and $z = d$. To $O(E)$, these introduce vertical velocities of

$$w = -\tfrac{1}{2}d E^{\frac{1}{2}}\zeta \quad \text{at } z = d, \tag{2.7}$$

and $$w - v \tan \beta = \tfrac{1}{2}d E^{\frac{1}{2}}\zeta \quad \text{at } z = y \tan \beta, \tag{2.8}$$

so that $\partial w/\partial z$ is given to within a similar error by

$$\frac{\partial w}{\partial z} = -\frac{v \tan \beta}{d} - E^{\frac{1}{4}}\zeta \tag{2.9}$$

in the main body of the flow. Neglecting other terms of $O(E)$ from (2.6), including the factor $Ro\zeta$ which introduces higher-order asymmetries into the flow, leads to the equation

$$\tau \frac{\partial \zeta}{\partial t} + \lambda \left(u \frac{\partial \zeta}{\partial x} + v \frac{\partial \zeta}{\partial y} \right) = -\zeta - \alpha v, \tag{2.10}$$

in terms of the two scaled parameters

$$\alpha = \frac{\tan \beta}{dE^{\frac{1}{2}}}, \quad \lambda = \frac{Ro}{2E^{\frac{1}{2}}}, \tag{2.11}$$

and the Ekman spin-up timescale $\tau = \frac{1}{2}E^{-\frac{1}{2}}$. The scaled vorticity equation (2.10) forms the basis of the present study, which aims to investigate the properties of the flow for any value of α and λ (given that the effect of τ is limited to a trivial scaling of t). In particular, note that the original four-parameter system has, in this context, been reduced to effectively a two-parameter system. As in Foster (1985), attention is restricted to the case of eastward flow ($\lambda > 0$) for which the bottom slopes upwards in the y-direction ($\alpha > 0$). This is geometrically similar to the westward-flow ($\lambda < 0$) case when $\alpha < 0$ but is fundamentally different from the other pair of possibilities (see, for example, Johnson & Page 1990).

As in previous studies, it is convenient for both the computation and presentation of the results to introduce a stream function ψ defined by

$$u = -\frac{\partial \psi}{\partial y}, \quad v = \frac{\partial \psi}{\partial x}, \tag{2.12}$$

in terms of which ζ can be written as

$$\zeta = \nabla^2 \psi, \tag{2.13}$$

where ∇^2 is the two-dimensional Laplacian. From (2.4), it follows that ψ is equal to $\frac{1}{2}P$ to leading order and so the streamlines represent lines of constant reduced pressure P. Together, the coupled equations (2.10) and (2.13) form the governing equations of the flow.

For the reasons outlined in the introduction, the obstacle selected for consideration in this paper is chosen to be cylindrical with a cross-section in the form of a symmetric Joukowski aerofoil (see figure 1). The half-width, $h_{\max}$ say, of this aerofoil is chosen to be approximately unity, in accordance with the non-dimensionalization above, and the half-length of the obstacle defined to be equal to L, which is generally an order one quantity in this study (the precise shape in terms of L is determined by the transformation given below). Note that the special case $L = 1$ corresponds to a circular obstacle while $L > 1$ corresponds to an aerofoil. For computational convenience, the channel is also considered to have a large finite width, equal to $2W$ far upstream and downstream, but slightly wider near the obstacle (see below). The Cartesian axes used to describe the flow are selected so that the aerofoil lies symmetrically about the line $y = 0$, between $x = -L$ and $x = L$. It is then straightforward to demonstrate that the resulting flow is symmetric about $y = 0$ to leading order, and so from this point only the flow for $y \geqslant 0$ will be considered. (Note that the asymmetries observed in experiments of Boyer & Davies (1982) can be attributed both to finite-Rossby-number effects, which are not present in the limit $Ro \to 0$ considered here, and to possible non-uniformities in the oncoming flow.)
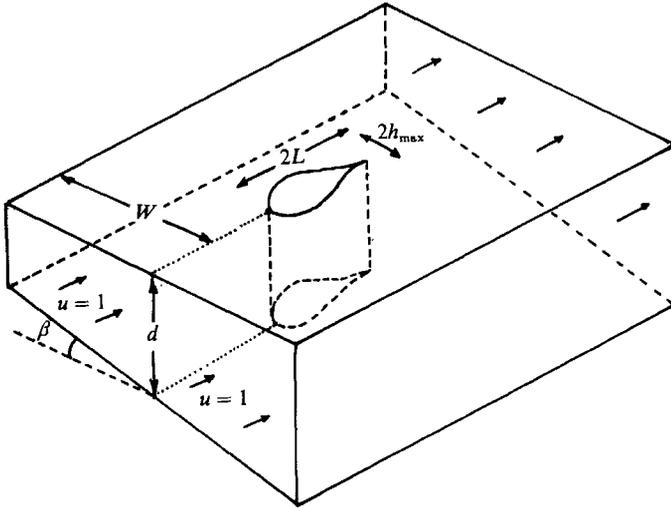
FIGURE 1. Schematic diagram illustrating the geometry and parameters used in this study (not drawn to scale). In this, and all subsequent figures, the flow is from left to right.

The boundary conditions applied on the flow field are that $\psi = 0$ on both the line of symmetry $y = 0$ and the aerofoil surface, and that $\psi = -W$ on the channel wall at $y \approx W$. This leads to a flow with an average streamwise velocity equal to one far upstream. The other boundary conditions imposed upstream on (2.10) and both upstream and downstream on (2.13) are discussed in §9 along with the numerical method. The initial condition on the vorticity, required by (2.10), is chosen to be identically zero, corresponding to flow started impulsively from rest.

For ease of computation, the flow region surrounding the Joukowski aerofoil can be transformed conformally into the upper half-plane by a mapping $z' = f(z)$, defined through

$$z' = \frac{1}{2}\left[\sigma + \frac{(L+1)^2}{\sigma}\right], \quad \sigma = z + 1 + \left(\left(z - \frac{1}{L}\right)^2 - \left(L - \frac{1}{L}\right)^2\right)^{\frac{1}{2}}, \quad (2.14)$$

where σ is a complex-valued variable, $z = x + iy$ is the complex number representation of a point in the original region, $z' = x' + iy'$ is the corresponding point in the transformed domain and the branch cut for the square root is a straight line joining the branch points $z = L$ and $z = 2/L - L$ (see, for example, Henrici 1974, p. 369). This mapping is defined so that the aerofoil is transformed into the line segment $|x'| \leqslant (L+1)$, $y' = 0$ and the line of symmetry is mapped into $|x'| \geqslant (L+1)$, $y' = 0$. As a result, the boundary condition $\psi = 0$ is applied on the complete line $y' = 0$ in the transformed region and, since $z' \sim z$ far from the obstacle, the uniform-flow condition in the new coordinates is $\psi \sim -y'$. For convenience, the boundary condition on the channel wall was applied on $y' = W$ so that, as mentioned above, the width of the flow domain is slightly larger than W near the obstacle.

As is common in experimental studies of geophysical flows, such as Boyer & Davies (1982), the sloping channel bottom is introduced because it has an effect which is similar to the so-called β-plane approximation. If instead the configuration were rotating at a rate $\frac{1}{2}(f^* + \beta^* y^*)$, in dimensional terms, then the resulting vorticity equation would be identical, to leading-order, to (2.10) but with $\tan \beta$ replaced by $\beta^* d^*/f^*$ and Ω^* replaced by $\frac{1}{2}f^*$ in (2.1).

3. The case $\lambda = 0$ with α arbitrary

In the limit as λ tends to zero, (2.10) reduces to the linear equation

$$\tau \frac{\partial \zeta}{\partial t} = -\zeta - \alpha \frac{\partial \psi}{\partial x}, \tag{3.1}$$

but, despite the relative simplicity of this, no analytical solutions are readily available except on an *f*-plane for which $\alpha = 0$ (and where ζ decays exponentially in t on a timescale of order τ). Once the flow becomes steady, however, ψ satisfies the second-order elliptic equation

$$\nabla^2 \psi + \alpha \frac{\partial \psi}{\partial x} = 0, \tag{3.2}$$

and some theoretical progress is possible in particular limits of α. This equation is identical to that derived by Foster (1985) for flow past a circular cylinder and an exact solution for α of $O(1)$ is presented in Johnson & Page (1990), using a similar expansion to that used for the contained flow in Hide & Hocking (1979).

The general properties of the flow in this parameter regime are similar to those described in each of the above papers. Of particular interest is the limit of flow as $\alpha \to \infty$, which Foster (1985) showed to have of a uniform velocity $(u, v) = (1, 0)$ in most of the channel, with streamlines following the lines of constant depth. The major exceptional region to this was upstream of the obstacle for values of y less than h_{max}, where the flow remained stagnant (as illustrated in figure 2 of his paper), although there were also two different types of thin shear layers, on the boundary of the stagnant region and on the downstream side of the obstacle. For $\alpha \gg 1$ these had thickness $O(1/\alpha^{\frac{1}{2}})$ and $O(1/\alpha)$ and contained velocities of $O(\alpha^{\frac{1}{2}})$ and $O(\alpha)$, respectively. Neither was due directly to viscous diffusion (since that effect was neglected from (2.10) under the limit $E \to 0$) but they were indirectly related to the effects of viscosity in the Ekman layers. Both types of layers, and a similar type of 'blocking' effect, were also present in the contained flow studied by Hide & Hocking (1979). As in that paper, it is clear that modifications to the structure outlined above are necessary once $\alpha = O(E^{-\frac{1}{4}})$, for E non-zero, in which case the layer of thickness $O(1/\alpha)$ is of the same thickness as the $E^{\frac{1}{4}}$ layer and (2.10) is inaccurate close to the obstacle. Since the limit $E \to 0$, with α and λ finite, is considered here, such modifications are not pursued in this paper.

The layers which appear upstream of the obstacle are governed, to leading order for $\alpha \gg 1$, by the parabolic equation

$$\frac{\partial^2 \psi}{\partial y^2} + \frac{\partial \psi}{\partial x} = 0 \tag{3.3}$$

and the appropriate solution to this, presented in Foster (1985), demonstrates that the layers are of thickness $O(|x|/\alpha)^{\frac{1}{2}}$ far upstream from the obstacle. Once $|x|$ is $O(\alpha)$, these layers near $y = \pm h_{max}$ merge together across the stagnant region to form a single region of width $O(1)$, within which the velocities are also $O(1)$. A solution for the flow in this region, obtained using Laplace transforms, is presented in equation (3.8) of Foster (1985), taking advantage of the fact that the obstacle in the scaled coordinates is effectively a transverse flat plate. A similar technique can be used for the flow considered in this paper, although the effect of the confining walls at $y \approx \pm W$
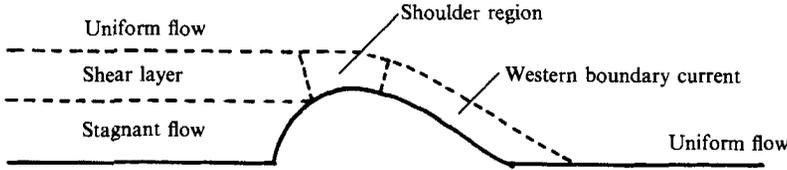
FIGURE 2. Schematic diagram illustrating the important flow regions for $\lambda = 0$ and $\alpha \gg 1$.

suggests that the general solution has the asymptotic form

$$\psi = -y + \sum_{n=1}^{\infty} A_n \exp\left(\frac{n^2\pi^2 x}{\alpha W^2}\right) \sin\frac{n\pi y}{W} \qquad (3.4)$$

far upstream. This solution demonstrates that as $|x|$ is increased the velocities tend exponentially towards the uniform flow $(u, v) = (1, 0)$, in constrast to Foster's solution for the semi-infinite flow which shows an algebraic decay towards the upstream boundary condition. In both cases, however, the stagnant, or 'blocked', flow is contained within a distance of $O(\alpha)$ upstream from the obstacle through frictional effects.

One of the important properties of these layers near $y = \pm h_{\max}$ is that they permit an $O(1)$ quantity of fluid to be transported around the stagnant region. This fluid is then carried into the second type of shear layer, which lies against the downstream side of the obstacle. Variously referred to as a 'western boundary current' or a Stommel layer (Pedlosky 1979), this region is confined to within a distance of $O(1/\alpha)$ of the downstream side of the obstacle when $\alpha \gg 1$ and its main role is to expel the aforementioned fluid into the outer uniform flow. Using a similar analysis to Foster (1985), an exact solution for the velocity in this layer can be calculated for an aerofoil obstacle and this is presented in §4 (where the $\lambda = O(1/\alpha)$ solutions are also considered).

The form of the flow for $\alpha \gg 1$ is shown schematically in figure 2, including the so-called 'shoulder' region (of size $\alpha^{-\frac{1}{3}} \times \alpha^{-\frac{2}{3}}$) described by both Foster (1985) and Hide & Hocking (1979). To illustrate the appearance of these features for large but finite values of α, (3.2) was solved numerically using the technique described in §9 and the streamlines for $\alpha = 32$ are illustrated in figure 3(a). Of particular note is the similarity in the features to those identified in figure 2. The vorticity ζ corresponding to the streamlines in figure 3(a) is plotted in figure 3(b) and this identifies more clearly the two types of thin shear layers described above, with the upstream shear layer extending over a distance of $O(\alpha)$ from the obstacle. This feature represents the archetype of upstream influence, where the effect of the obstacle is 'felt' by the fluid before it reaches there, a phenomenon which forms an important part of not only this study but also related work in both stratified fluids (Baines 1977) and axial flow in a rotating fluid (Stewartson 1958).

The mechanism through which the effect of the obstacle can extend far upstream is apparent from the unsteady form of (3.1), since $\alpha \gg 1$, the Rossby-wave solutions of

$$\tau\frac{\partial \zeta}{\partial t} + \alpha\frac{\partial \psi}{\partial x} = 0 \qquad (3.5)$$

are able to propagate throughout the flow domain. Given any non-equilibrium initial flow, waves are subsequently generated at the obstacle and these propagate away in all directions, eventually leaving behind a steady flow like that illustrated in figure 3 for $\alpha = 32$. To illustrate why the final steady solution has this particular form an
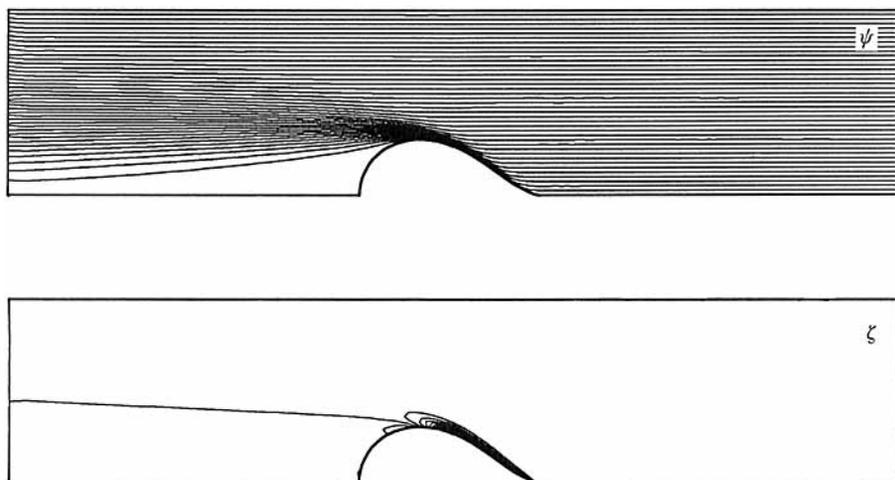
FIGURE 3. Numerical solutions for the flow when $\lambda = 0$ and $\alpha = 32$, showing (a) the stream function ψ (with contour interval $\Delta\psi = 0.1$) and (b) the corresponding vorticity ζ (with contour interval $\Delta\zeta = 10$).

equivalent argument to that in Lighthill (1967) can be invoked, using the well-known result that the dispersion relation for Rossby waves with $\psi \propto \exp[\mathrm{i}(kx + ly - \omega t)]$ is

$$\omega\tau = \frac{-\alpha k}{k^2 + l^2}. \tag{3.6}$$

Thus the phase of these waves always moves towards the negative x-direction while the group velocity

$$c_{\mathrm{g}} = \frac{\alpha}{\tau(k^2 + l^2)^2}(k^2 - l^2, 2kl) \tag{3.7}$$

can be directed in either the upstream or the downstream directions, depending on the wavenumber (k, l) of the disturbance component. As a result, once waves have propagated away from the obstacle, the only remaining components in the steady flow are those with $k = 0$ and, since the x-component of c_{g} is always negative in this case, these appear only on the upstream side of the obstacle. The amplitudes of the disturbance components for each wavenumber l is then such that together they exactly balance the uniform oncoming flow for $y < h_{\mathrm{max}}$, forming into the 'blocked' region described above.

For $O(1)$ values of α the flow has broadly the same properties as would be expected from the structure outlined above for $\alpha \gg 1$. In particular, the numerical results illustrated in figure 4 for various values of α show a region of retarded flow ahead of the obstacle, although it is not completely stagnant. This is bounded by a 'tongue' of vorticity which extends upstream from the obstacle peak, over a distance which is broadly proportional to α. Also apparent in figure 4 is the high-vorticity region against the downstream side of the obstacle, which becomes thinner and stronger as α is increased. Since the contour interval chosen for each of the vorticity plots in figure 4 is proportional to the value of α used, it is clear that the vorticity induced in the upstream region is roughly proportional to α and that the vorticity in the 'western boundary current' increases more rapidly than α. This is consistent with the asymptotic theories for these layers when $\alpha \gg 1$, described above. The major dynamical difference between the flows for $\alpha \gg 1$ and for $\alpha = O(1)$ arises through the
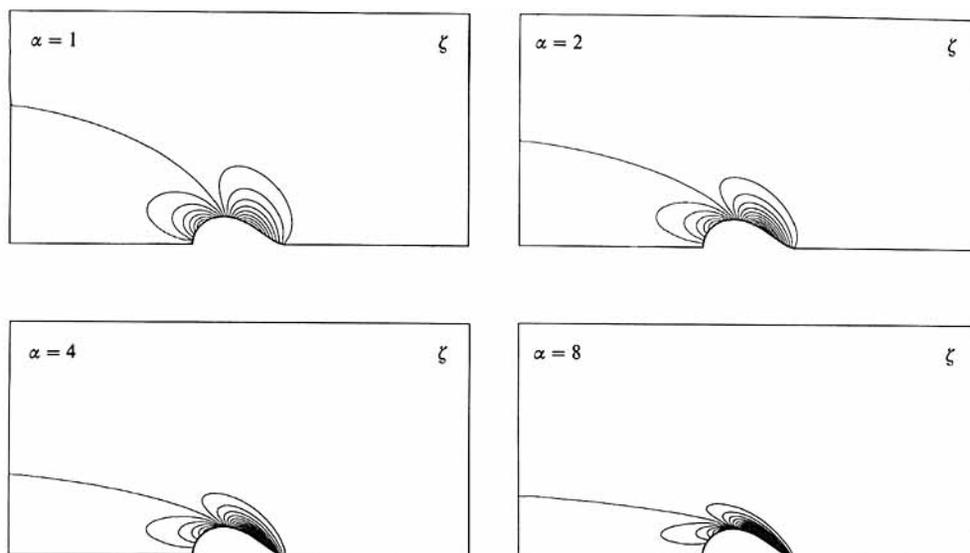
FIGURE 4. Numerical solutions showing the vorticity ζ (with contour interval $\Delta\zeta = 0.1\alpha$) for $\lambda = 0$ and $\alpha = 1$, 2, 4 and 8, plotted over the range $-10 \leqslant x \leqslant 10$. These values lie along cross-section A on figure 9.

term $-\zeta$ in (3.1) which has a frictional effect on the flow (see also Page 1987), so that thin shear layers are smeared out and Rossby waves are dissipated more strongly where this term is relatively important.

Most of the structure described above remains valid for small non-zero values of λ, provided that $\lambda \ll 1$ when $\alpha = O(1)$ and $\lambda \ll 1/\alpha$ when $\alpha \gg 1$. Further details of the case where $\lambda = O(1/\alpha)$ are presented in both Johnson & Page (1990) and the following section of this paper.

4. The case $\lambda = O(1/\alpha)$ when $\alpha \gg 1$

As λ is increased from zero, the first nonlinear modifications to the $\alpha \gg 1$ flow described in §3 occur once λ reaches $O(1/\alpha)$, at which stage the flow in both the 'western boundary current' and 'shoulder' regions is modified from the $\lambda = 0$ structure. Proposals for the modification to the equations in these regions for a flow past a circular cylinder were presented in §4 and §5 of Foster (1985), however there were some difficulties in the details of these proposals which are clarified in the companion to this paper, Johnson & Page (1990). It is therefore worth indicating here how they relate to the flow past an aerofoil.

First, the general solution of (2.10) for $\lambda = 0$, in terms of the transformed coordinates (x', y') described in §2, satisfies

$$Q^2\left(\frac{\partial^2\psi}{\partial x'^2} + \frac{\partial^2\psi}{\partial y'^2}\right) + \alpha\left(\frac{\partial x'}{\partial x}\frac{\partial\psi}{\partial x'} + \frac{\partial y'}{\partial x}\frac{\partial\psi}{\partial y'}\right) = 0, \qquad (4.1)$$

where $Q = |df/dz|$ is the stretching factor introduced by the transformation. To examine the layer of thickness $O(1/\alpha)$ against the downstream side of the aerofoil the scaled coordinate $\bar{y}' = \alpha y'$ can be introduced and for $\alpha \gg 1$ it follows that

$$Q^2\frac{\partial^2\psi}{\partial\bar{y}'^2} + \frac{\partial y'}{\partial x}\frac{\partial\psi}{\partial\bar{y}'} = 0 \qquad (4.2)$$

in this region, where Q and $\partial y'/\partial x$ are now evaluated on $y' = 0$. Both Q and $\partial y'/\partial x$ can be evaluated in terms of the inverse $z = g(z')$ of the transformation $z' = f(z)$, for $-(L+1) \leqslant x' \leqslant (L+1)$, and the boundary condition $\psi \sim -y$ at the outer edge of the layer can be written as $\psi \rightarrow -h(x')$ as $\bar{y}' \rightarrow \infty$, where $h(x')$ is the aerofoil height at x' (given by the imaginary part of $g(x')$). Equation (4.2) can then be integrated exactly to give the solution

$$\psi = -h\left[1 - \exp\left(\frac{\mathrm{d}h}{\mathrm{d}x'}\bar{y}'\right)\right], \tag{4.3}$$

which is similar to (4.6) in Foster (1985) (for direct comparison with that result it can be shown that $h = \sin\theta$ and $\mathrm{d}h/\mathrm{d}x' = -\frac{1}{2}\cot\theta$, in terms of his variable θ, for $L = 1$). For the aerofoil flow, as for the circular cylinder, $\mathrm{d}h/\mathrm{d}x'$ is zero at the peak of the obstacle and less than zero on the downstream side and therefore the 'western boundary current' layer can only exist for $x_0' \leqslant x' \leqslant (L+1)$, where x_0' is the point where h is maximum. Unlike the circular cylinder case, $\mathrm{d}h/\mathrm{d}x'$ approaches zero at the trailing edge of the aerofoil (rather than becoming infinite), but this presents no real difficulties since the layer contains no fluid at that point. In figure 5, the scaled tangential velocity $\bar{u}' = -Q\,\partial\psi/\partial\bar{y}'$ on $\bar{y}' = 0$ is plotted, based on the solution (4.3), and it is significant to note that on the $\lambda = 0$ curve $\bar{u}'$ vanishes at both the peak and trailing edge of the aerofoil, with $\bar{u}' \propto (L+1-x')^2$ in the latter case (as can be verified from (4.3)).

As λ is increased from zero to $O(1/\alpha)$, for $\alpha \gg 1$, the nonlinear terms in the western boundary current become important and (4.2) no longer accurately describes the flow. The equation governing $\bar{u}'$ then becomes

$$\bar{\lambda}Q^2\left(\frac{\partial\psi}{\partial x'}\frac{\partial\bar{u}'}{\partial\bar{y}'} - \frac{\partial\psi}{\partial\bar{y}'}\frac{\partial\bar{u}'}{\partial x'}\right) + \bar{u}' + \frac{\mathrm{d}h}{\mathrm{d}x'}Q(\psi+h) = 0, \tag{4.4}$$

in terms of $\bar{\lambda} = \lambda\alpha$, equivalent to (4.1) in Foster (1985). Replacing $\bar{y}'$ by a stream function coordinate ψ, this equation can be written as

$$\bar{\lambda}Q\bar{u}'\frac{\partial\bar{u}'}{\partial x'} + \bar{u}' + \frac{\mathrm{d}h}{\mathrm{d}x'}Q(\psi+h) = 0, \tag{4.5}$$

and the solutions of this have similar properties to those described by Foster (1985) for the circular cylinder, except that there is no critical value of $\bar{\lambda}$ beyond which a similarity solution exists at the trailing edge (because $Qh\,\mathrm{d}h/\mathrm{d}x'$ decreases to zero quadratically, rather than linearly, near that point). Since (4.5) is nonlinear and Q and h are all complicated functions of x', no exact solutions of (4.5) are available and therefore the equation was integrated numerically over the range $x_0' \leqslant x' \leqslant (L+1)$, starting with the initial condition $\bar{u}' = 0$ at $x' = x_0'$. These numerical solutions, obtained using centred-difference approximations, are plotted on figure 5 for the single streamline $\psi = 0$. For small values of $\bar{\lambda}$ the velocity falls to zero quadratically at the trailing edge, as it does for $\bar{\lambda} = 0$. However, for values of $\bar{\lambda}$ larger than about 1.74 (when $L = 2$), and in particular $\bar{\lambda} = 2$, 4 and 8 shown in figure 5, the velocity on the $\psi = 0$ streamline is not zero at the trailing edge and instead, through (4.5), it satisfies the condition $\bar{\lambda}Q\,\partial\bar{u}'/\partial x' = -1$ at that point (which is, incidentally, the usual separation condition for $E^{\frac{1}{4}}$ layers). The appearance of non-zero velocities at the trailing edge is similar to that noted by Foster for his $\bar{\lambda} > \frac{1}{4}$ solutions, but in this case it is not accompanied by the development of a singularity at the end of the layer since there is no difficulty in having non-zero tangential velocities at the trailing edge of
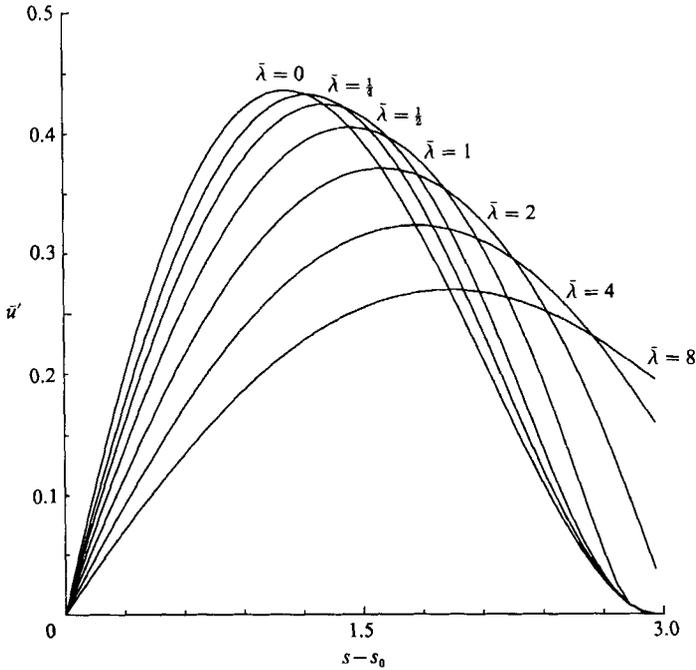
FIGURE 5. The scaled tangential velocity $\bar{u}'$ against the surface of the obstacle for the case when $\bar{\lambda} = \lambda\alpha$ is $O(1)$ and $\alpha \gg 1$. The velocity is plotted for several values of $\bar{\lambda}$ and the distance s is measured around the obstacle from the front stagnation point, with $s = s_0$ at the obstacle peak.

the aerofoil. In contrast, at the rear stagnation point of the cylinder the same property would violate the symmetry condition $v = 0$ on $y = 0$ and lead to the development of a complicated asymptotic structure (Johnson & Page 1990; Page & Johnson 1990). In confirmation of this, numerical solutions to the full equations (examined in §10) show that there is change in the form of the $\alpha = 16$ solutions near the trailing edge at a value of $\bar{\lambda}$ between 1 and 2 when $L = 2$, with a jet-like feature appearing in the wake near $y = 0$. This appears to correspond to the 'southern boundary layer' described in Johnson & Page (1990) and the entrained fluid is eventually carried back into the western boundary current via a 'return shear layer' (see also Page & Johnson 1990). No inertial turning region is needed in this case.

The form of the solutions near the outer edge of the layer, where $\psi \approx -h$ and $\bar{u}'$ is small, is also of interest. Approximating (4.4) in this region, ψ satisfies

$$\bar{\lambda}Q^2 \frac{\mathrm{d}h}{\mathrm{d}x'} \frac{\partial^2\psi}{\partial\bar{y}'^2} - \frac{\partial\psi}{\partial\bar{y}'} + \frac{\mathrm{d}h}{\mathrm{d}x'}(\psi + h) = 0, \qquad (4.6)$$

and this has solutions of the form $\psi = -h + A\exp{(c\bar{y}')}$, with c given by

$$c = \frac{1 \pm (1 - 4\bar{\lambda}Q^2(\mathrm{d}h/\mathrm{d}x')^2)^{\frac{1}{2}}}{2\bar{\lambda}Q^2(\mathrm{d}h/\mathrm{d}x')}. \qquad (4.7)$$

Since $\mathrm{d}h/\mathrm{d}x'$ is negative, it is apparent that both of these values of c are negative and furthermore that, for $\bar{\lambda}$ sufficiently large, they are complex-valued (with a negative real part) at some points along the aerofoil. In Foster's case this occurs first at the rear stagnation point, when $\bar{\lambda} = \frac{1}{4}$, but for the aerofoil the occurrence of complex values of c, and hence an oscillatory flow at the outer edge of the layer, appears first

in the vicinity of the minimum of $\mathrm{d}h/\mathrm{d}x'$. As a result the 'spiralling' solutions, encountered by Foster near the rear stagnation point, do not present difficulties near the trailing edge of an aerofoil obstacle. More generally, it can be shown that the spiralling solutions will be present at the rear stagnation point of bodies with a bluff trailing edge when $\bar{\lambda} > \frac{1}{4}$, but that they are never present at the end of bodies with a sharp 'cusped' trailing edge, on which $Q\mathrm{d}h/\mathrm{d}x' \to 0$ as $x' \to (L+1)$. A body with a finite-angled wedge at the rear provides a transition between these two cases, with a critical value of $\bar{\lambda} = 1/(4\sin^2\gamma)$ for the existence of spiralling solutions, where γ is the half-angle of the wedge. Note that for large values of $\bar{\lambda}$ the imaginary part of c is proportional to $1/\bar{\lambda}^{\frac{1}{2}}$, and hence the wavelength of the oscillations in this layer is $O(\lambda/\alpha)^{\frac{1}{2}}$ in the unscaled coordinates, while the real part of c is proportional to $1/\bar{\lambda}$, which corresponds to a decay scale of $O(\lambda)$. These two features are consistent with those discussed, more generally, in the following two sections.

5. The case $\alpha \gg 1$ with λ arbitrary

In each of the previous sections it was apparent that the flow upstream of the obstacle is modified with the formation of an upstream blocked region extending over distances of order α when α is large. Scaling (2.10) into this region by introducing a new variable $\bar{X} = x/\alpha$, it follows that

$$\frac{\lambda}{\alpha}\left(\frac{\partial\psi}{\partial\bar{X}}\frac{\partial}{\partial y} - \frac{\partial\psi}{\partial y}\frac{\partial}{\partial\bar{X}}\right)\frac{\partial^2\psi}{\partial y^2} + \frac{\partial\psi}{\partial\bar{X}} + \frac{\partial^2\psi}{\partial y^2} = 0 \tag{5.1}$$

so that while λ of $O(1)$ an equivalent leading-order equation to (3.3) is recovered. Solutions to this equation therefore have the same series form (3.4), except that for large n the nonlinear term in (5.1) cannot be neglected in comparison to the other terms. As a guide to the modifications which arise in this case, (5.1) has exact solutions of the form

$$\psi = -y + F_n \sin\frac{n\pi y}{W}, \tag{5.2}$$

provided
$$F_n(\bar{X}) \propto \exp\left(\frac{(n\pi)^2\bar{X}}{W^2 - \lambda(n\pi)^2/\alpha}\right). \tag{5.3}$$

This same modal solution also satisfies the linearized equation, which is appropriate when $u \approx 1$ and $v \approx 0$, and so a general series solution of a similar form to (3.4) can be found far upstream, but with the exponential variation in x replaced by (5.3) and the summation truncated beyond the largest integer N less than $(\alpha/\lambda)^{\frac{1}{2}}W/\pi$. This solution remains valid far upstream for larger values of λ, up to and including $O(\alpha)$, although the sum contains at most an $O(1)$, rather than an $O(\alpha^{\frac{1}{2}})$, set of terms in that case. For smaller values of λ, in particular when λ is $O(1/\alpha)$ as in the previous section, the same argument demonstrates that only the highest wavenumber components are absent from the upstream flow, and so the qualitative features of the flow are unlikely to be altered significantly from those described in §3 for $\lambda = 0$. For increasing λ the sharpness of the boundary between the stagnant and uniform flow regions in figure 2 is lost, both through the absence of the higher wavenumbers and the nonlinearity of the shear layer between those regions.

The solution (5.3) also demonstrates that wave components with $n > N$ decay downstream and can therefore only appear behind the obstacle in the steady flow. For $n \approx N$ these modes have a wavelength in y of order $(\lambda/\alpha)^{\frac{1}{2}}$ so that for λ of $O(1/\alpha)$

they can be identified with the waves in the 'Rossby layer' discussed in the previous section. Furthermore, (5.3) demonstrates that they decay over a lengthscale of $O(\lambda)$, and both of these properties are consistent with the conclusions of §4, based on the form of the flow near the outer edge of the western boundary current for $\lambda = O(1/\alpha)$. As a result, the streamlines can be expected to show a relatively large number of these oscillations, of short wavelength, extending downstream of the obstacle for λ of $O(1)$ and $\alpha \gg 1$. This represents a considerable modification to the structure in §4 where the jet emanating from the upstream shear layer is confined to within a 'western boundary current' close to the obstacle.

Whether oscillations of a certain wavelength appear upstream or downstream in the steady flow can also be determined using a group velocity argument similar to that outlined for $\lambda = 0$ in §3. For non-zero λ an additional term appears in the dispersion relation (3.6) for Rossby waves far upstream, so that

$$\omega\tau = \lambda k - \frac{\alpha k}{k^2 + l^2} \tag{5.4}$$

when the velocity (u, v) is close to $(1, 0)$. The x-component of $\boldsymbol{c}_{\mathrm{g}}$ then becomes

$$c_{\mathrm{g}x} = \frac{\lambda}{\tau} + \frac{\alpha(k^2 - l^2)}{\tau(k^2 + l^2)^2} \tag{5.5}$$

and the steady $k = 0$ components will only travel upstream while $l^2 < \alpha/\lambda$, equivalent to the condition $n < N$ above. In contrast, the higher-wavenumber components have $c_{\mathrm{g}x} > 0$ and they therefore appear downstream in the steady flow. In addition to these $k = 0$ components, (5.4) also suggests that steady wave modes with $k^2 + l^2 = \alpha/\lambda$ can exist (as in Lighthill 1967) and these appear downstream of the obstacle (since $c_{\mathrm{g}x} > 0$) and produce the 'lee-wave train' examined in §6. These waves did not appear from the analysis based on (5.1) and (5.3) since their lengthscale is generally shorter than $O(\alpha)$.

6. The case $\lambda = O(\alpha)$ when $\alpha \gg 1$

The next regime in which some theoretical progress can be made is for a steady flow with $\alpha \gg 1$ and $\lambda = O(\alpha)$, under which the Ekman suction term can be neglected from the vorticity equation in most of the flow and (2.10) approximated by

$$\lambda \left(u \frac{\partial \zeta}{\partial x} + v \frac{\partial \zeta}{\partial y} \right) = -\alpha v. \tag{6.1}$$

This equation is well known (see, for example, Pedlosky 1979), and it follows that the quantity $\mathscr{F} = (\lambda\zeta + \alpha y)$, often known as the 'potential vorticity', is conserved along streamlines. Since $\mathscr{F}$ is a function of ψ only then its value is fixed by the potential vorticity at any point on each streamline (for example far upstream), and ζ can be determined everywhere in the flow field by the relation

$$\lambda\zeta + \alpha y = \mathscr{F}(\psi). \tag{6.2}$$

Using (2.13), this can be written as an elliptic equation for ψ, which is generally nonlinear but can, in principle, be solved given appropriate boundary conditions on ψ. Despite this apparent reduction in the complexity of the problem, solving for the

resulting flow does present some practical difficulties; in particular, the appropriate function $\mathscr{F}(\psi)$ and the appropriate boundary conditions on ψ are not always readily identifiable.

As an example of this, consider the particular case when $\mathscr{F}$ is linear; exact solutions of (6.2) are then relatively easy to calculate and they have been given for several different cases of flow past obstacles by Long (1955), Miles (1968), Huppert & Miles (1969) and Miles & Huppert (1968, 1969). (Later studies by McCartney (1975) and Johnson (1977, 1978) extended this work to flow above topography in a similar configuration.) The key assumption behind the choice of a linear $\mathscr{F}$ is that the flow is undisturbed and uniform far upstream, so that $\psi \to -y$ and $\zeta \to 0$ as $x \to -\infty$, and, through (6.2), ψ satisfies the linear equation

$$\nabla^2 \psi + \frac{\alpha}{\lambda} \psi = -\frac{\alpha}{\lambda} y \tag{6.3}$$

along all streamlines originating from upstream. Homogeneous solutions of (6.3) are wavelike in character and the studies mentioned above chose, based on energy arguments, solutions for which no standing waves were present in front of the obstacle for $x^2 + y^2 \gg 1$ (this is possible through an appropriate choice of boundary conditions on ψ for $x < 0$ far from the obstacle, using an argument like that in §7 of Lighthill 1966). The resulting flows were plotted (for example, in the Appendix of Miles & Huppert, 1968) for several values of a parameter κ, equal to $(\alpha/\lambda)^{\frac{1}{2}}$ in this context, and it was found that solutions with u positive everywhere could only be found for certain values of κ (the vanishing of u was identified with a loss of static stability in their context). For a finite-depth fluid this requires that κ be away from certain 'resonant' values (Long 1955), while for semi-infinite fluid κ should be less than a single critical value (close to 1.27 for the circular obstacle). Despite this, consistent solutions could be calculated for other values of κ although in some cases the flow developed closed-streamline regions, with not all streamlines originating from upstream (thereby invalidating (6.3) in those regions). As a result, the correct steady flow corresponding to an initially-uniform upstream profile can probably only be calculated either by solving an unsteady initial-value problem or by introducing viscous effects. Pursuing the former, it becomes apparent that, through analogous arguments to those in Stewartson (1958), the flow evolves towards an equilibrium state through the generation of Rossby waves which can propagate both upstream and downstream of the obstacle. In particular, the waves can modify the oncoming profile to form a 'blocked' region such as that seen in §3 (an extreme case for which the oncoming profile is modified to $u = 0$ for $y < 1$). Of course, the same argument also applies to the flows without closed streamlines calculated by Long and Miles, and hence even those flows do not necessarily correspond to an initially-uniform upstream profile.

A similar problem has been examined experimentally in the analogous stratified-flow case by Baines (1977) where the assumption of an undisturbed upstream flow profile was also shown to be inappropriate for the same reasons. In that case it was likewise shown that, under suitable conditions, internal waves could propagate upstream of the obstacle and that these would modify the upstream profile which remains once the equilibrium state is reached. This provides some experimental verification for the type of process described above, albeit in a different configuration.

From the above it can be concluded that, except under special initial conditions, $\mathscr{F}$ will not be a linear function of ψ. Despite this, by assuming that the inflow is dominated by a uniform flow in the x-direction, some useful information can be
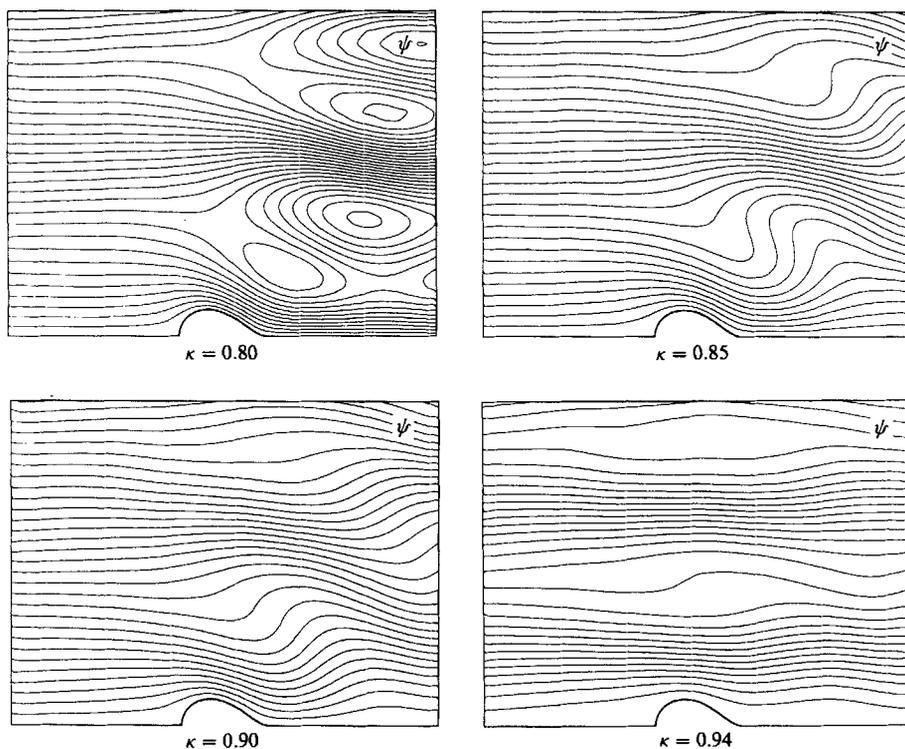
FIGURE 6. Numerical solutions for the streamlines calculated using 'Long's model' for flow past an aerofoil in a channel of width $W = 20$, at several values of $\kappa = (\alpha/\lambda)^{\frac{1}{2}}$ when $\lambda \gg 1$ (with contour interval $\Delta\psi = 0.5$).

gained by using (6.3) in an approximate sense. In particular, a number of observed features of the flow for $\alpha \gg 1$ can be identified, for example solutions to the homogeneous form of (6.3) will have wavenumber of magnitude $|k| = (\alpha/\lambda)^{\frac{1}{2}}$ and wavelength $2\pi/|k|$. Also, the magnitude of the forcing terms on the right-hand side of (6.3) indicates that the vorticity ζ generated over the obstacle will be $O(\alpha/\lambda)$. Both of these features are apparent in the solutions plotted in figure 6 and in the numerical results presented in §10.

Apart from the calculation of an appropriate $\mathscr{F}$, another difficulty with the so-called 'Long's model' concerns the appropriate specification of the boundary conditions on ψ for the elliptic equation (6.2). As noted above, Miles & Huppert assumed that 'no stationary waves are present in front of the obstacle' for $x^2 + y^2 \gg 1$, and chose their Green function solutions of (6.3) accordingly. However, that condition is not in a form which is readily applicable to solutions of (6.3) in regions for which the appropriate Green function is not available. In practice it is simpler to use a more-general approach which is applicable to numerical calculations, so the method chosen in this study was first to solve the non-homogeneous equation (6.3) with arbitrarily-specified boundary conditions and then subtract appropriate multiples of the complementary functions to eliminate any stationary waves in the oncoming profile. Solutions of the nonlinear equation (6.2) could also be calculated using a similar process at each step of a Newton iteration.

Using the method described above, numerical solutions of (6.3) were calculated and the stream function plots for these are shown in figure 6 for several values of

$\kappa = (\alpha/\lambda)^{\frac{1}{2}}$. As pointed out in the Appendix of Miles & Huppert (1968), the upper boundary has a marked influence on the flow, particularly for smaller values of κW, and so the same value $W = 20$ was used as for the solutions to be presented in §10. Based on the theory for $L \gg 1$ in Long (1955), it is apparent that u can vanish within the flow and that closed streamlines can be present when κW is close to an integer multiple of π, due to a 'resonance' effect. Figure 6 illustrates the same effects for a short obstacle. Resonance for mode 5 occurs at $\kappa = 0.25\pi \approx 0.785$ and for mode 6 at $\kappa = 0.30\pi \approx 0.942$. The strongest distortions occur just above resonance (here mode 5) becoming weaker as the wavenumber increases and remaining small extremely close to, but just less than, the next resonance (here mode 6). Whether the wavenumber lies above or below a resonant wavenumber appears more important in determining the strength of the lee-wavefield for Long's model than the exact distance of the flow from resonance. It is shown in §10 that the numerical solutions to the complete problem do not display this behaviour and thus it appears that the extremes of overturning are a consequence of the assumption of no upstream influence.

The evolution of the flow for long obstacles, with $L \gg 1$, near resonance in stratified flow has been reduced to the solution of a forced Korteweg–de Vries equation by Grimshaw & Smyth (1986), and the necessity of upstream influence demonstrated in this case. Similar analysis for the flow on a β-plane produces the same conclusion (R. H. J. Grimshaw & E. R. Johnson, private communication).

7. The case $\lambda \gg 1$ with α arbitrary

Despite the large value of λ in the parameter regime considered above, the influence of Ekman suction does become significant far from the obstacle. A similar effect is clear in previous studies of flows past obstacles on an f-plane, for example Page (1983, 1987), where the same term leads to a decay of vorticity along streamlines over a lengthscale of $O(\lambda)$ from the obstacle. To examine the effect of this term, a scaled variable $X = x/\lambda$ can be introduced so that for $\lambda \gg 1$ (2.10) becomes, to leading order,

$$\left(\frac{\partial \psi}{\partial X}\frac{\partial}{\partial y} - \frac{\partial \psi}{\partial y}\frac{\partial}{\partial X}\right)\frac{\partial^2 \psi}{\partial y^2} + \frac{\alpha}{\lambda}\frac{\partial \psi}{\partial X} + \frac{\partial^2 \psi}{\partial y^2} = 0. \tag{7.1}$$

This is equivalent to equation (5.1) introduced on the $O(\alpha)$ lengthscale in §5 and, assuming that u is close to unity, solutions of this equation can be sought of the same form (5.2), yielding

$$F_n(X) \propto \exp\left(\frac{(n\pi)^2 X}{(\kappa W)^2 - (n\pi)^2}\right). \tag{7.2}$$

In fact, this solution is identical to (5.3) when expressed in terms of x and so, as before, F grows exponentially with X when $\kappa W > n\pi$ and decays exponentially in X when $\kappa W < n\pi$. Modes with $n < \kappa W/\pi$ are therefore found only upstream in the steady solution and the modes with $n > \kappa W/\pi$ are found only downstream, with both sets of modes decaying away from the obstacle. Thus, for fixed κ, whether a mode appears upstream or downstream is not affected by dissipation (i.e. the value of λ). When more than one mode is present, either upstream or downstream, the sum of the modes is not a solution of the full nonlinear equation (7.1), but a similar argument can still be applied for each mode in a linearized sense far from the obstacle.

From (7.2) it is apparent that the most slowly decaying component of the upstream solution has an e-folding length of $(\alpha W^2/\pi^2 - \lambda)$, so that its extent increases as α is increased (for fixed λ) and decreases as λ is increased, when α is held fixed. Once $\lambda > \alpha W^2/\pi^2$, however, no steady waves can exist upstream and (7.2) implies that the nth mode on the downstream side of the obstacle decays over a lengthscale of $(\lambda - \alpha W^2/n^2\pi^2)$. This is largest when n is large and gives an e-folding length of λ in the downstream direction.

8. The case $\alpha \ll 1$ with λ arbitrary

The $\alpha = 0$, or f-plane, case has been studied extensively in the literature (see, for example, Page (1987) for a review of this work). In this section the case of a flow with an arbitrary value of λ is considered but with α small, so that the effects of the bottom slope introduce only a small perturbation upon the f-plane flow. The first step in the calculation of this flow is to find the steady solution for $\alpha = 0$, identified here with a zero subscript. From (2.10) this satisfies

$$\lambda \left(u_0 \frac{\partial \zeta_0}{\partial x} + v_0 \frac{\partial \zeta_0}{\partial y} \right) = -\zeta_0, \tag{8.1}$$

and, using coordinates which follow the streamlines of the flow, it is apparent that the vorticity ζ_0 decays exponentially along streamlines, over a lengthscale of $O(\lambda)$. For a uniform flow which enters upstream of the obstacle it then follows that $\zeta_0 = 0$ everywhere in the flow domain, and ψ_0 satisfies

$$\nabla^2 \psi_0 = 0. \tag{8.2}$$

In terms of the conformally-mapped coordinates (x', y') introduced in §2, the exact solution to (8.2) is simply $\psi_0 = -y'$ and this can be expressed in terms of x and y by evaluating the imaginary part of z' in (2.14).

Having calculated the solution ψ_0 for $\alpha = 0$, it is possible to calculate the leading-order correction for $\alpha \ll 1$ by expanding ψ and ζ in powers of α, in the form

$$\psi = \psi_0 + \alpha\psi_1 + \alpha^2\psi_2 + \dots, \quad \zeta = \zeta_0 + \alpha\zeta_1 + \alpha^2\zeta_2 + \dots. \tag{8.3}$$

Substituting these into (2.10), ζ_1 satisfies

$$\lambda \left(u_0 \frac{\partial \zeta_1}{\partial x} + v_0 \frac{\partial \zeta_1}{\partial y} \right) = -\zeta_1 - v_0, \tag{8.4}$$

and for $\lambda = 0$ the solution $\zeta_1 = -\partial\psi_0/\partial x$ is plotted in figure 7 (a). The corresponding stream function perturbation ψ_1 can be found exactly in terms of an integral by solving the Poisson equation $\nabla^2\psi_1 = \zeta_1$ in the z'-plane (although in this study the equation was integrated numerically) to give the streamlines illustrated in figure 7 (b). One feature of particular interest in perturbation stream function ψ_1 is the pair of recirculating cells which act to decrease the speed of the flow close to the obstacle on the upstream side, and increase its speed in the corresponding downstream position. This could be interpreted as a weak form of the upstream-blocking effect described in §3, although in this case it is not due to stationary Rossby waves upstream of the obstacle (since $\kappa \ll 1$).

For non-zero λ the perturbation vorticity cannot be evaluated directly from (8.4) but some theoretical progress is possible if that equation is written in terms of
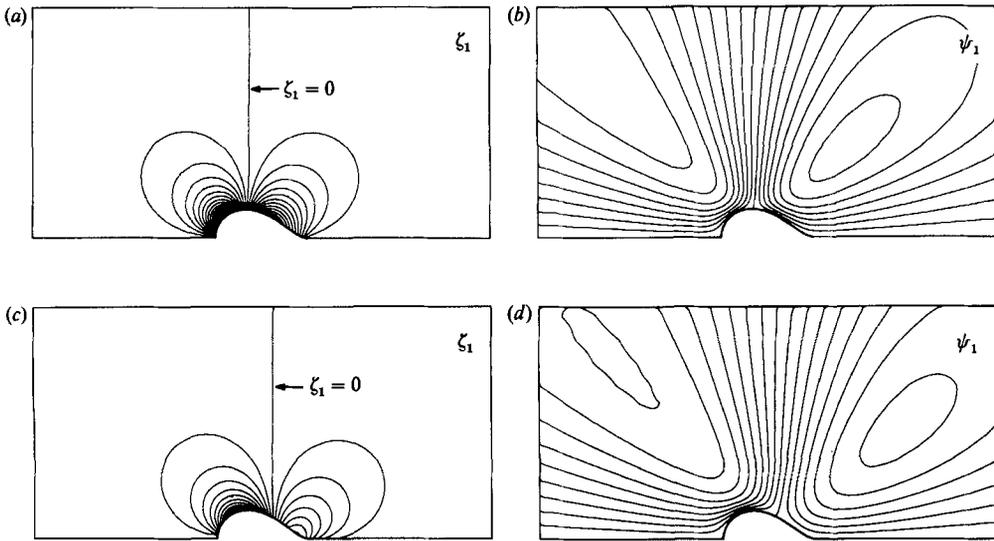
FIGURE 7. (a) The vorticity perturbation ζ_1 induced when $\lambda = 0$ and $\alpha \ll 1$ (with $\Delta\zeta = 0.05$), (b) the corresponding perturbation stream function ψ_1 (with $\Delta\psi = 0.05$), (c) ζ_1 for $\lambda = 1$, (d) the corresponding ψ_1.

coordinates which follow the leading-order streamlines $\psi_0 = $ constant. Since these streamlines are along the lines with y' constant here, the equation for ζ_1 becomes

$$\lambda Q^2 \frac{\partial \zeta_1}{\partial x'} = -\zeta_1 - v_0, \tag{8.5}$$

where $Q = |df/dz|$ is the speed of the leading-order flow. The normal y' to each streamline does not appear explicitly in this equation and so it can be integrated with respect to x' and, assuming that ζ_1 is (at most) finite far upstream, the solution can be written in the form

$$\zeta_1 = -\int_{-\infty}^{x'} v_0 \exp\left(-\int_{x_1'}^{x'} \frac{dx_2'}{\lambda Q^2}\right) \frac{dx_1'}{\lambda Q^2}. \tag{8.6}$$

For small λ this reduces to $\zeta_1 \approx -v_0$, while for larger values of λ the integral can be interpreted as an average over upstream values of $-v_0$, with an exponential weighting towards the values within $O(\lambda)$ of x'. Thus inertial effects introduce a 'delay' in the response of the vorticity to upstream changes in v_0 and skew the vorticity field in the downstream direction, as shown for $\lambda = 1$ in figure 7(c). This leads to a corresponding skewing of the perturbation stream function field ψ_1, as shown in figure 7(d).

Of some interest is the flow along the streamline $\psi_0 = 0$, which extends around the obstacle and follows the line of symmetry $y = 0$ both upstream and downstream of the obstacle. In front of the obstacle v_0 is equal to zero on this streamline, and so $\zeta_1 = 0$, but once the streamline begins to follow the obstacle surface v_0 becomes positive and negative values of ζ_1 are generated. For $\lambda > 0$ these negative values persist beyond the point where v_0 changes sign, and as λ increases further the point where ζ_1 becomes positive approaches the trailing edge of the obstacle. In contrast to the flow when $\lambda = 0$, there is no reason in this case why the integral for ζ_1 should
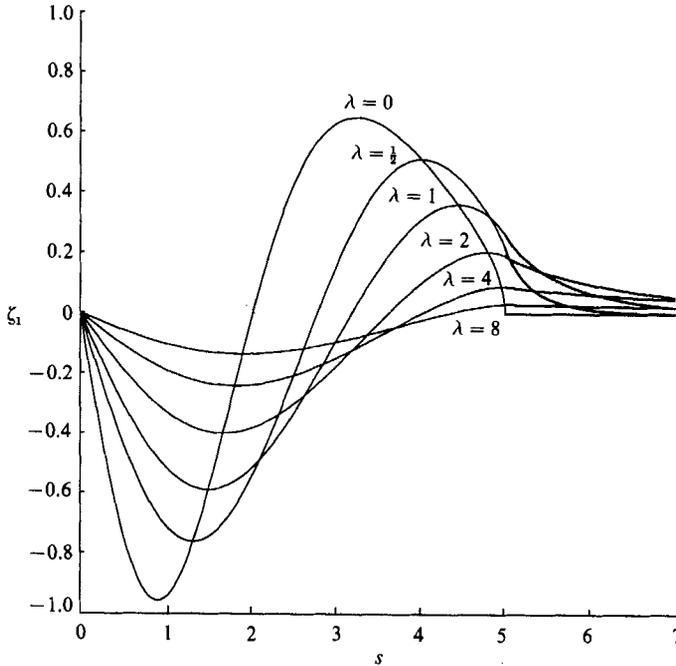
FIGURE 8. Numerical solutions for the perturbation vorticity ζ_1 on the surface of the obstacle for $\alpha \ll 1$ and various values of λ. The distance s is measured as in figure 5 except that calculations continue beyond the trailing edge and into the wake.

return to zero at the trailing edge and so a wake is generated which contains a non-zero jump in vorticity across $y = 0$ (since $v_0 = 0$ in this wake, its strength decays exponentially over a lengthscale of $O(\lambda)$ downstream of the obstacle). All of these features are apparent in figure 8, where a numerical solution of (8.5), obtained using the Runge–Kutta method in the z'-plane, has been plotted for several values of λ. The observed decrease in strength of the vorticity around the obstacle as λ is increased can be shown directly from (8.6), since ζ_1 is of $O(1/\lambda)$ when $\lambda \gg 1$.

For obstacles with a bluff trailing edge, such as a circular cylinder, there is no vorticity discontinuity across and wake and ζ_1 approaches zero in a singular region, containing large vorticity gradients, near the trailing edge. In particular, solving (8.5) along the surface of a circular cylinder implies that $\zeta_1 \propto \theta^{1/2\lambda}$, where $\theta \ll 1$ is the angle measured from the rear stagnation point. This leads to numerical difficulties when solving the equations by finite differences, which is a further reason for the choice of an aerofoil-shaped obstacle in this study.

9. Numerical method

Together, the governing equations (2.10) and (2.13) form a pair of coupled nonlinear equations for ζ and ψ. Given ψ, (2.10) is essentially a first-order hyperbolic equation for ζ, the solution of which is determined uniquely by specifying ζ as a function of time across the upstream boundary. Given ζ, (2.13) is a Poisson equation for ψ, and its solution is unique once appropriate boundary conditions for ψ have been specified on $y = 0$, the aerofoil, $y \approx W$ and both the upstream and downstream boundaries.

To facilitate a numerical solution, the domain described in §2 was first transformed conformally into a simpler rectangular domain using the mapping $z' = f(z)$ described in (2.14). In this transformed plane, (2.10) and (2.13) can be written as

$$\tau \frac{\partial \zeta}{\partial t} + Q^2 \left(\frac{\partial \psi}{\partial x'} \frac{\partial}{\partial y'} - \frac{\partial \psi}{\partial y'} \frac{\partial}{\partial x'} \right) (\lambda \zeta + \alpha y) = -\zeta, \tag{9.1}$$

and

$$Q^2 \nabla'^2 \psi = \zeta, \tag{9.2}$$

where, as before, $Q = |df/dz|$ is the local stretching factor introduced by the transformation. The resemblance of these equations to their original form is a further advantage of this type of transformation.

As mentioned in §2, the upper boundary of the computational domain was chosen to follow the curve $y' = W$, rather than $y = W$, and consequently the channel wall was slightly wider in the region of the obstacle than at the upstream and downstream boundaries (despite this the channel boundary was generally within 1% of the line $y = W$). The upstream and downstream boundaries were likewise chosen to correspond to constant values of x' (rather than x), but since they were generally located far from the aerofoil this presented no difficulties. Consequently, the computational domain was rectangular in the (x', y')-plane and so the boundary conditions on both (9.1) and (9.2) were relatively easy to apply. Furthermore, the finite-difference forms of $\partial/\partial x'$ and $\partial/\partial y'$ could be evaluated easily at gridpoints located along the lines of constant x' and y' with no special treatment necessary near the obstacle.

To evaluate (9.1) and (9.2) numerically, central differences were used for both $\partial/\partial x'$ and $\partial/\partial y'$ except on the boundaries where second-order one-sided differences were used. To help resolve features near the aerofoil, the gridlines on which the equations were evaluated were spaced unevenly so that there was a concentration of points near both $x' = \pm(L+1)$ and $y' = 0$. For all of the calculations presented in this paper 150 points were used in the x'-direction, typically between $x' = -40$ and $x' = 20$, with 50 points used in the y'-direction. Also, for most calculations presented here W was chosen equal to 20 and L equal to 2.

The equations were integrated in time using a modified ADI method, similar to that described for the interior flow in Page (1982), which linear stability analysis indicates is stable for any choice of timestep. However, in practice the method failed to converge for larger values of Δt, and so typically $\Delta t = 0.05\tau/\alpha$ was used for most of the calculations presented in this paper. Integrations of (9.1) and (9.2) were iterated at least twice within each timestep and the calculations generally continued until the maximum value of $\tau \partial \psi/\partial t$ was less than 0.1% of the steady ψ field. The Poisson equation (9.1) was solved using an efficient cyclic-reduction routine at each iteration (Swarztrauber 1974).

After the calculations were completed in the z'-plane, the results were transformed back into the z-plane using the inverse transformation $z = g(z')$ of (2.14), defined by

$$z = \frac{1}{2} \left[\left(\sigma - \frac{L+1}{L} \right) + \frac{(L - (1/L))^2}{(\sigma - (L+1)/L)} \right] + \frac{1}{L}, \quad \sigma = z' + (z'^2 - (L+1)^2)^{\frac{1}{2}}, \tag{9.3}$$

where σ is the same complex-valued variable as used in (2.14) and the branch cut of the square root in the z'-plane extends between $-(L+1)$ and $(L+1)$.

One of the difficulties encountered in the study was the choice of appropriate boundary conditions on ψ and ζ. For a uniform flow far upstream from the obstacle the appropriate boundary condition on (2.10) is to require that $\zeta \to 0$ as $x \to -\infty$,
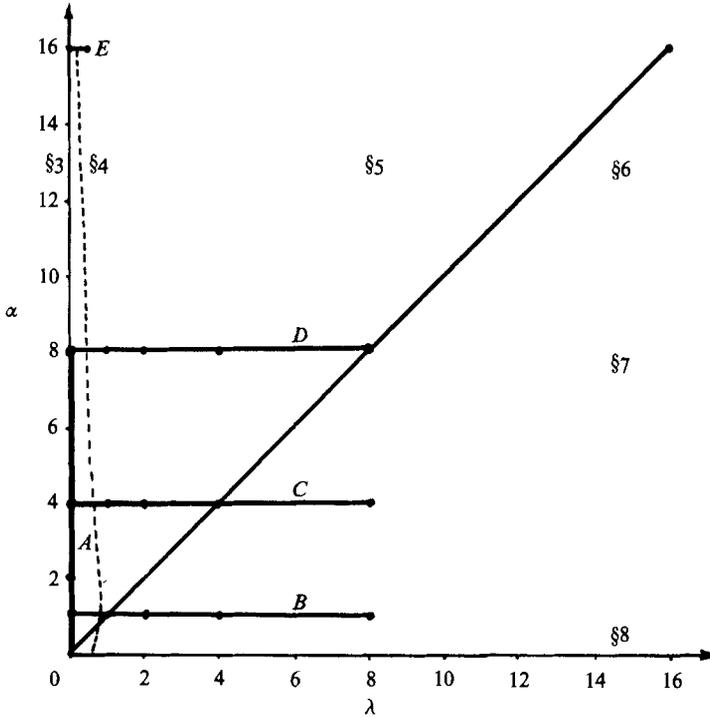
FIGURE 9. A diagram of (α, λ) parameter space illustrating the broad asymptotic regions examined in §§3–8, along with the cross-sections referred to in §10. The critical values of λ above which $E^{\frac{1}{4}}$-layer separation may occur is identified by the broken line.

however, owing to the relatively slow upstream decay in some cases (particularly when α is large), a radiation-type boundary condition with

$$\frac{\partial \zeta}{\partial t} + \left(\lambda - \frac{\alpha W^2}{\pi^2}\right)\frac{\partial \zeta}{\partial x'} + \zeta = 0 \tag{9.4}$$

is more appropriate, with the bracketed term set to zero when it is positive. This condition enables the slowest decaying mode, identified in §7, to proceed out of the upstream boundary and, provided it is imposed sufficiently far upstream of the obstacle, it should have little effect on the remaining modes (in practice, the differences obtained by applying this, rather than $\zeta = 0$, are minimal except close to the boundary). The boundary conditions on the Poisson equation present further difficulties because they require the specification of ψ (or its normal derivative) on both the upstream and downstream boundaries. On the upstream boundary an equivalent condition to (9.4) was used on the deviations of the stream function from the uniform flow, $\psi + y'$, while on the downstream boundary it was assumed that the flow decayed exponentially towards a uniform flow with a lengthscale of λ, as determined in §7. Therefore the condition

$$\frac{\partial \psi}{\partial t} + \lambda \frac{\partial \psi}{\partial x'} + \psi + y' = 0 \tag{9.5}$$

was applied at a distance large compared with both the length of the obstacle and λ, although in practice these conditions often produced similar results to those obtained with the simpler condition $\partial \psi / \partial x' = 0$ at the same boundaries.

10. Numerical results for $\alpha = O(1)$ and $\lambda = O(1)$

For $O(1)$ values of both α and λ, the vorticity equation (2.10) is nonlinear with no known exact solutions available, and so the features of the flow in this regime can only be examined by calculating numerical solutions of (2.10) and (2.13). Despite this, the theories outlined for each of the asymptotic cases in §§3–8 give a good indication of many of the qualitative features of the flows in this regime, and so in this section the numerical results will be examined to determine the ways in which these features are combined and are modified beyond the regimes in which they are strictly valid. Numerical calculations were performed for a number of different cross-sections of the two-dimensional parameter space (α, λ), each of which are illustrated on figure 9. Also shown on figure 9 are the broad regions representing the range of parameters for which the asymptotic theories described in §§3–8 are applicable, as well as the values for which a viscous flow might be expected to separate (see §11).

The first cross-section, marked A on figure 9, was considered in §3 where the flow for $\lambda = 0$ was examined. In particular, the vorticity ζ for this case is shown in figure 4 at various values of α, and the presence of both the upstream 'blocked' region, of length $O(\alpha)$ when $\alpha \gg 1$, and the 'western boundary current' region, of thickness $O(1/\alpha)$, were noted earlier and so will not be discussed further here.

The second cross-section, marked B, considers the flow for $\alpha = 1$, and a selection of vorticity contour plots calculated on this line at several values of λ are shown in figure 10. Although this choice of parameters does not strictly lie within the $\alpha \ll 1$ region considered in §8, several of the features of the flow observed in that asymptotic case are evident in these plots. In particular, for $\lambda = 1$ the vorticity plot shows some similarities to that shown in figure 7(c), the leading term in a series expansion for small α, with the $\zeta = 0$ contour extending from close to the peak of the obstacle and separating the upstream region negative vorticity from the positive values downstream. Another common feature is the manner in which the magnitude of the vorticity decreases away from the obstacle surface, on which the extrema of ζ are attained. As λ is increased, the vorticity plots in figure 8 indicate that the $\zeta = 0$ line leaves the obstacle from a point further downstream from the peak and, in fact, that this point approaches the trailing edge of the obstacle as $\lambda \to \infty$. This feature is also clear in figure 10, as is the decreasing rate of decay of vorticity in the wake as λ is increased (in contrast to the upstream decay of ζ which appears to be much less affected by the value of λ). As a broad summary, it can be concluded that increasing λ increases the advection in the streamwise direction and tends to reduce vorticity differences between parts of the flow along the same streamline.

However, there are some differences between the trends in figure 10 and the flow predicted on the basis of the theory in §8. For example, the vorticity distribution in figure 7 becomes skewed downstream with increasing λ whereas that in figure 10 is skewed upstream for all λ. An indication of this is provided by the $\zeta = 0$ contour marked on figure 10. In addition, an isolated region of weak negative vorticity is present behind the obstacle in figure 10, corresponding to where v becomes positive again behind the obstacle, but this feature is not present in figure 7. These differences can be ascribed to the absence of Rossby waves (represented by the interaction between the $-\alpha v$ and the terms in (8.1)) in the perturbation solution and hence the lack of any form of upstream effect or lee waves.

The stream function plots for each of the cases shown in figure 10 show only relatively small differences from the potential-flow solution. However, if α is increased to 4 and various values of λ are considered then some trends in the plots
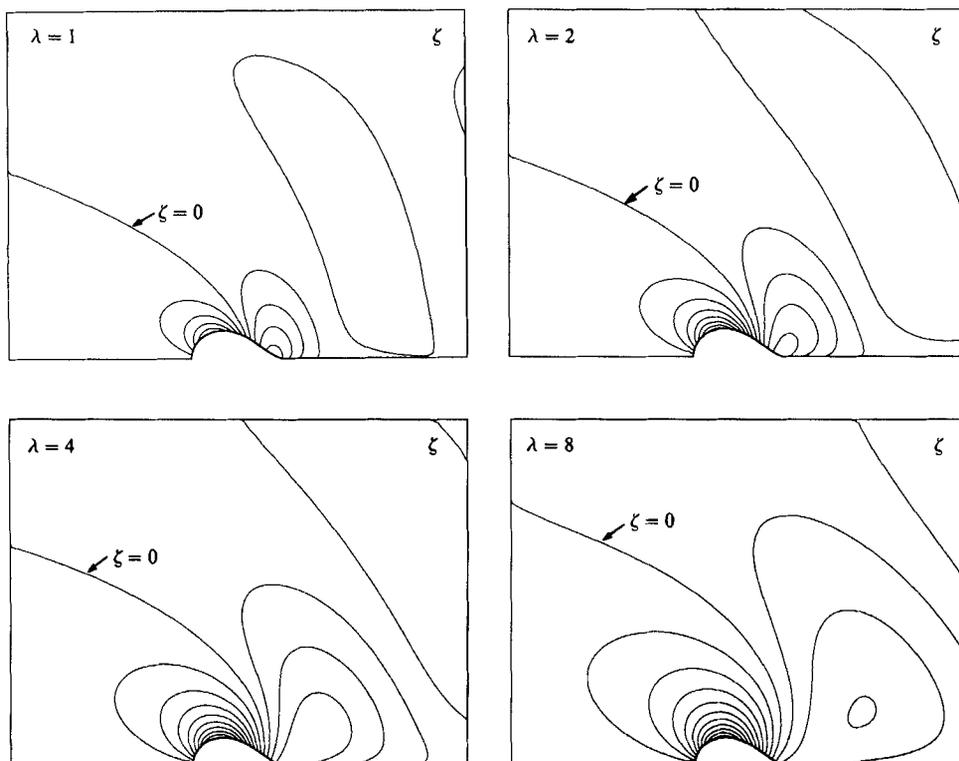
FIGURE 10. Numerical solutions showing the vorticity ζ (with contour interval $\Delta\zeta = 0.1/\lambda$) for $\alpha = 1$ and $\lambda = 1, 2, 4$ and 8, corresponding to cross-section B on figure 9. In this and most subsequent plots, only the $-10 \leqslant x \leqslant 10$ portion of the computational domain is shown.

of ψ do become apparent. To illustrate these, the vorticity is plotted for cross-section C in figure 11(a) and the most obviously different feature from figure 10 is the oscillatory wake extending downstream at an angle of about 45° to the x-axis (this angle is fairly insensitive to λ but does increase gradually with α). The corresponding feature in the streamline plots in figure 11(b) is a waviness in the streamlines, or a 'lee-wavetrain', rather like those shown in figure 6. Consistent with the asymptotic results in §6, the wavelength of these waves increases with λ but their strength, as represented by the amplitude of the streamline displacements, decreases in inverse proportion to λ. Also consistent is the lengthscale over which these waves decay downstream, demonstrated to be $O(\lambda)$ when $\lambda \gg 1$ in §7. In contrast, the lengthscale of the upstream effect has increased in figure 11, in comparison with the same λ values in figure 10, but as λ is increased for any particular α this lengthscale decreases again. This is also in accordance with the predictions in §7.

For large values of α similar features to those noted above remain, but with the wavelength of the lee waves decreasing (for the same value of λ) and the magnitude of the corresponding streamline displacements increasing (roughly in proportion to α/λ for $\lambda \geqslant O(1/\alpha)$). However, in addition to these features, two of the characteristics of the $\lambda = 0$ flow, examined in §3, also become more apparent. These are the upstream effect, which was seen in §7 to have decay scale $(\alpha W^2/\pi^2 - \lambda)$, so that its extent increases as α is increased, and the 'western boundary current' which gets thinner for larger α. To illustrate these features, a third cross-section (marked D on figure 9), was calculated and the numerical results for this are illustrated in figure 12.
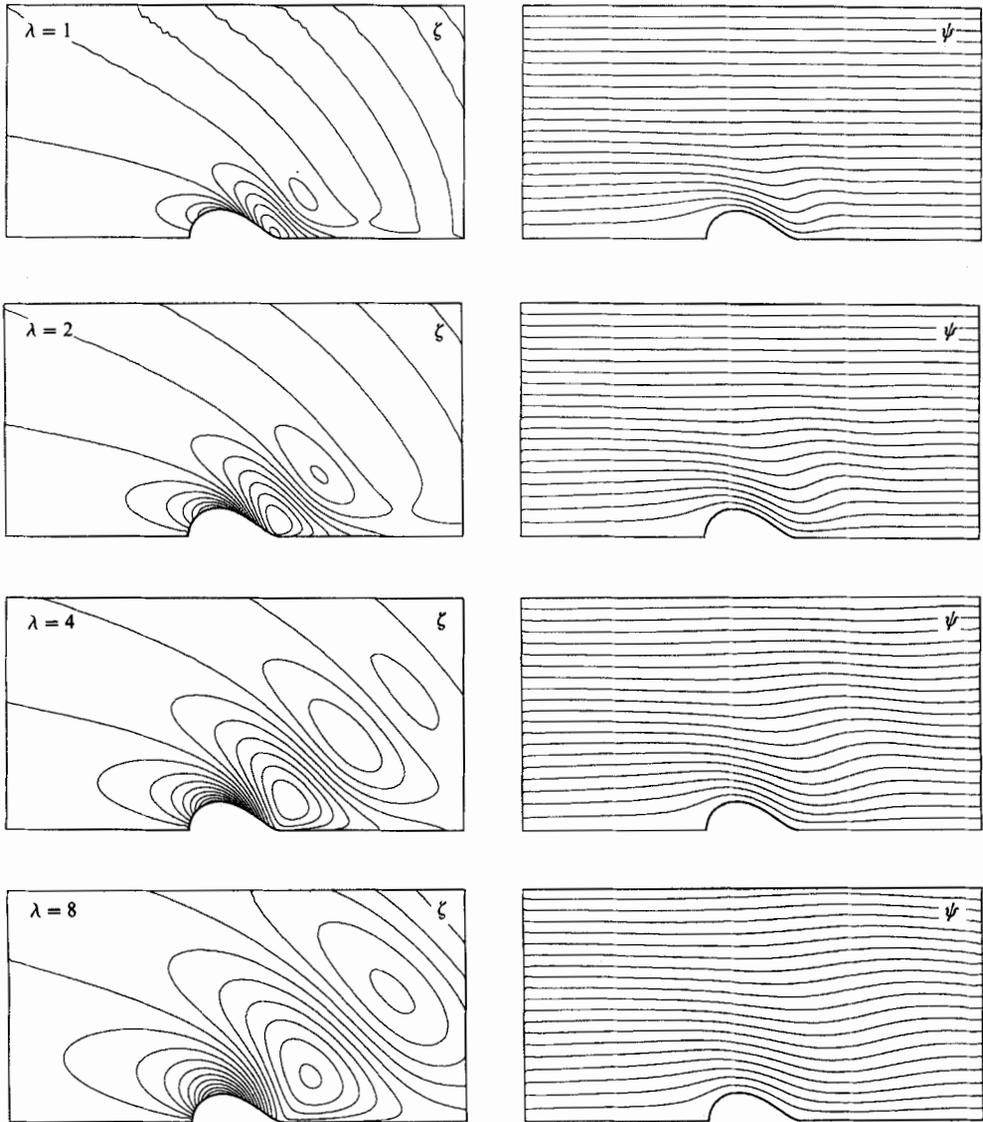
FIGURE 11. Numerical solutions showing (a) the vorticity ζ (with $\Delta\zeta = 0.4/\lambda$) and (b) the stream function ψ (with $\Delta\psi = 0.5$) for $\alpha = 4$ and $\lambda = 1, 2, 4$ and 8. These values correspond to cross-section C on figure 9.

The upstream blocking effect is discernable in the $\lambda = 1$ plot but is most obvious in plots of the flow speed (not shown here). Note, in particular, that the condition $\alpha > \lambda l^2$ for the existence of steady upstream modes is satisfied for between six and eighteen wave components in these plots, so that some upstream influence is certainly present. Also apparent by comparing figure 11 and figure 12 is that the velocities against the downstream side of the obstacle increase with α, for fixed λ, and the thickness of the western boundary current shrinks in the same limit (in accordance with the $\lambda = 0$ case in §3); this results in a stronger lee-wavefield at the larger α value. The strengthening of the lee waves can also be explained through the approximate conservation of potential vorticity, as represented in (6.3), since the forcing to that equation is proportional to α/λ.
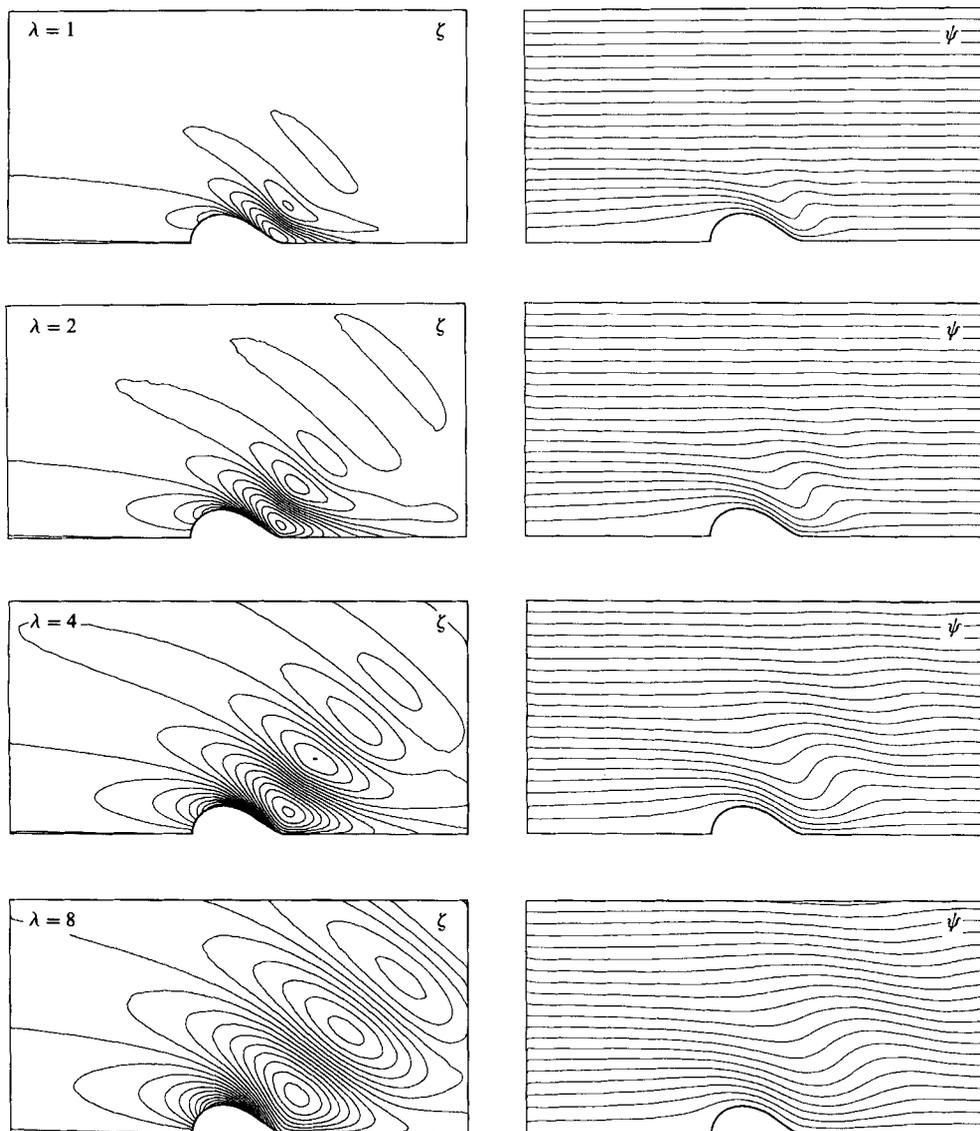
FIGURE 12. Numerical solutions showing (a) the vorticity ζ (with $\Delta\zeta = 0.8/\lambda$) and (b) the stream function ψ (with $\Delta\psi = 0.5$) for $\alpha = 8$ and $\lambda = 1, 2, 4$ and 8. These values correspond to cross-section D on figure 9.

Of particular interest is the case when the wavelength of the lee waves is of the same magnitude as the thickness of the western boundary current at large values of α. This regime corresponds to that examined both in Foster (1985) and in §4, and the region of most interest is against the downstream surface of the obstacle. As a result several streamline plots for the cross-section E are shown in figure 13, restricted to the region $0 \leqslant x \leqslant 4$, at four different values of $\bar{\lambda} = \lambda\alpha$ (note that a finer grid spacing was used near $y' = 0$ for these calculations). These streamlines represent the solutions of the full equations (2.10) and (2.13) and it is clear that, although there are thin regions of high shear, there is no short-scale region in which the flow must turn by 180°, as would be expected for a cylindrical obstacle from the analysis of Foster (1985). Of particular note is the thin jet-like flow which leaves the surface of the
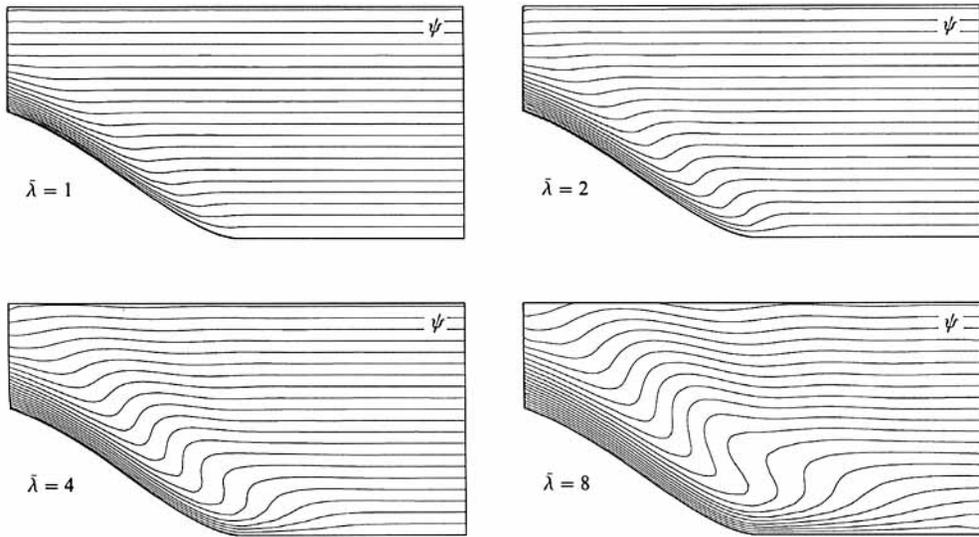
FIGURE 13. Numerical solutions showing the stream function ψ for $\alpha = 16$ and $\bar{\lambda} = 1, 2, 4$ and 8, plotted over the range $0 \leqslant x \leqslant 4$ and using the contour interval $\Delta\psi = 0.1$. These values correspond to cross-section E on figure 9.

obstacle at the trailing edge, with the streamlines then returning to their appropriate y-level after travelling a relatively short distance in the wake. This retention of fluid at the end of the 'western boundary current' for larger values of $\bar{\lambda}$ is a feature of the asymptotic theory in §4, but no detailed theory of the trailing-edge region is proposed here. Preliminary calculations with a circular cylindrical obstacle show highly singular behaviour at the rear stagnation point in this regime, in contrast to the smooth behaviour as the flow leaves the rear of the aerofoil, and this is consistent with the behaviour of a western boundary current near a corner (Page & Johnson 1990).

The final cross-section shown on figure 9, marked F, is of particular relevance to the asymptotic theory described in §6, for which the 'potential vorticity' $\mathscr{F} = (\lambda\zeta + \alpha y)$ is conserved along streamlines. For this cross-section λ is kept equal to α, and several values of α are considered for the results shown on figure 14. The largest value of λ used is 16, giving a decay scale roughly equal to the width of the computational region shown, yet the lee waves have considerably smaller amplitudes and the vorticity is much weaker than in the corresponding Long's model plot for $\kappa = 1$ (also shown). While both dissipative and upstream effects are absent from the Long's model calculations, the results in figure 14 seem to indicate that the major differences are due to the latter effect. As a further illustration of this, plots of the stream function are shown in figure 15 at three values of κ, based on both the numerical results for $\lambda = 16$ and the Long's model calculation. The numerical results vary smoothly and almost imperceptibly, showing a slight increase in lee-wave strength with increasing κ, consistent with the asymptotic result that the maximum vorticity is proportional to κ^2. In Long's model mode 6 is resonant for $\kappa = 0.30\pi \approx 0.942$ and mode 7 for $\kappa = 0.35\pi \approx 1.10$. The pattern for $\kappa = 0.95$ lies just above a resonance and so has a highly distorted lee-wavefield entirely absent from the numerical results. The patterns further above resonance have lee-wavefields weaker than the almost-resonant field but still stronger than the lee-waves in the numerical results and more slowly decaying away from the obstacle. This strongly supports the
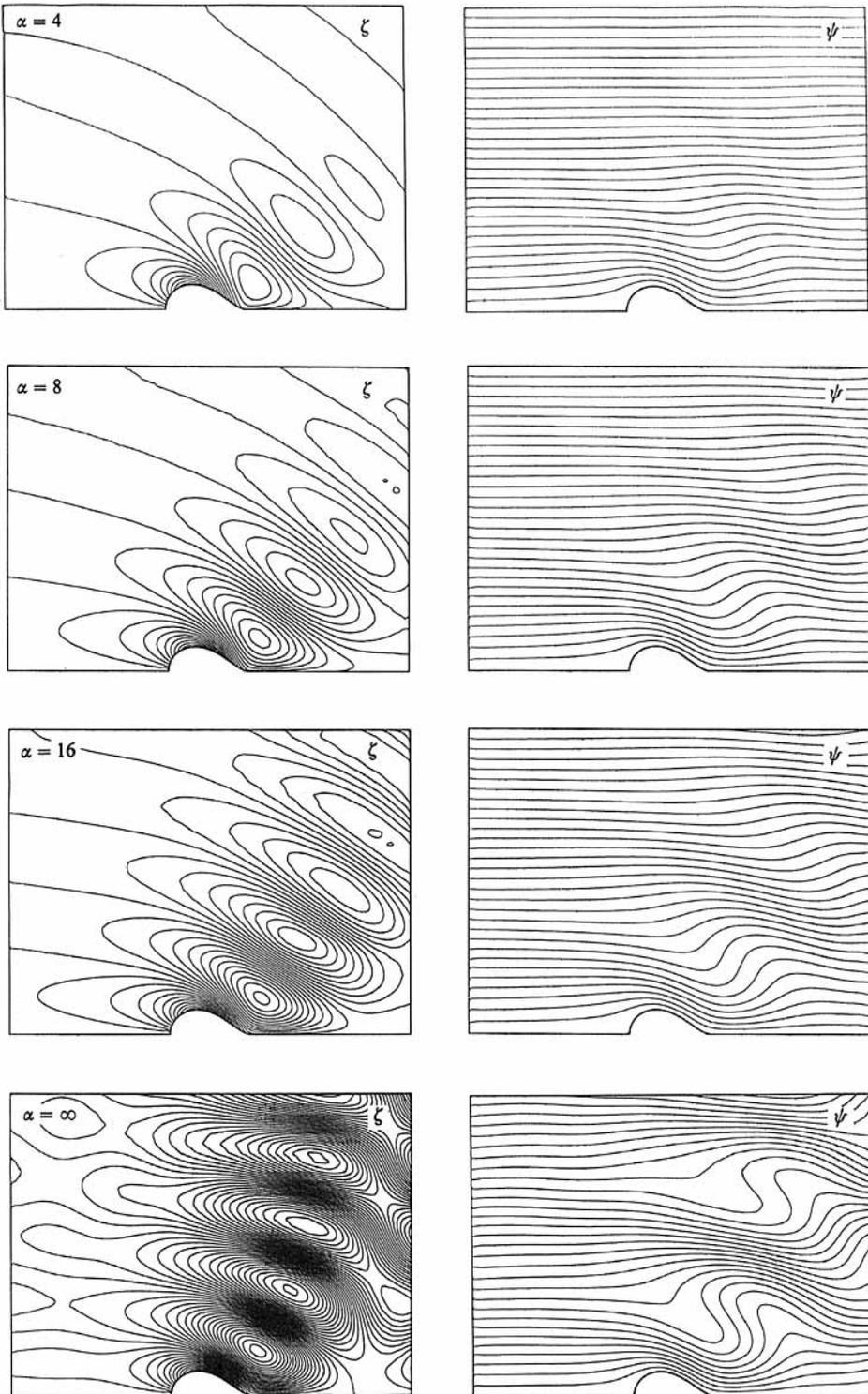
FIGURE 14. Numerical solutions showing (*a*) the vorticity ζ (with $\Delta\zeta = 0.1$) and (*b*) the stream function ψ (with $\Delta\psi = 0.5$) for $\lambda = \alpha$ and $\alpha = 4$, 8 and 16, along with a Long's model solution for $\kappa = 1$. These values correspond to cross-section F on figure 9.
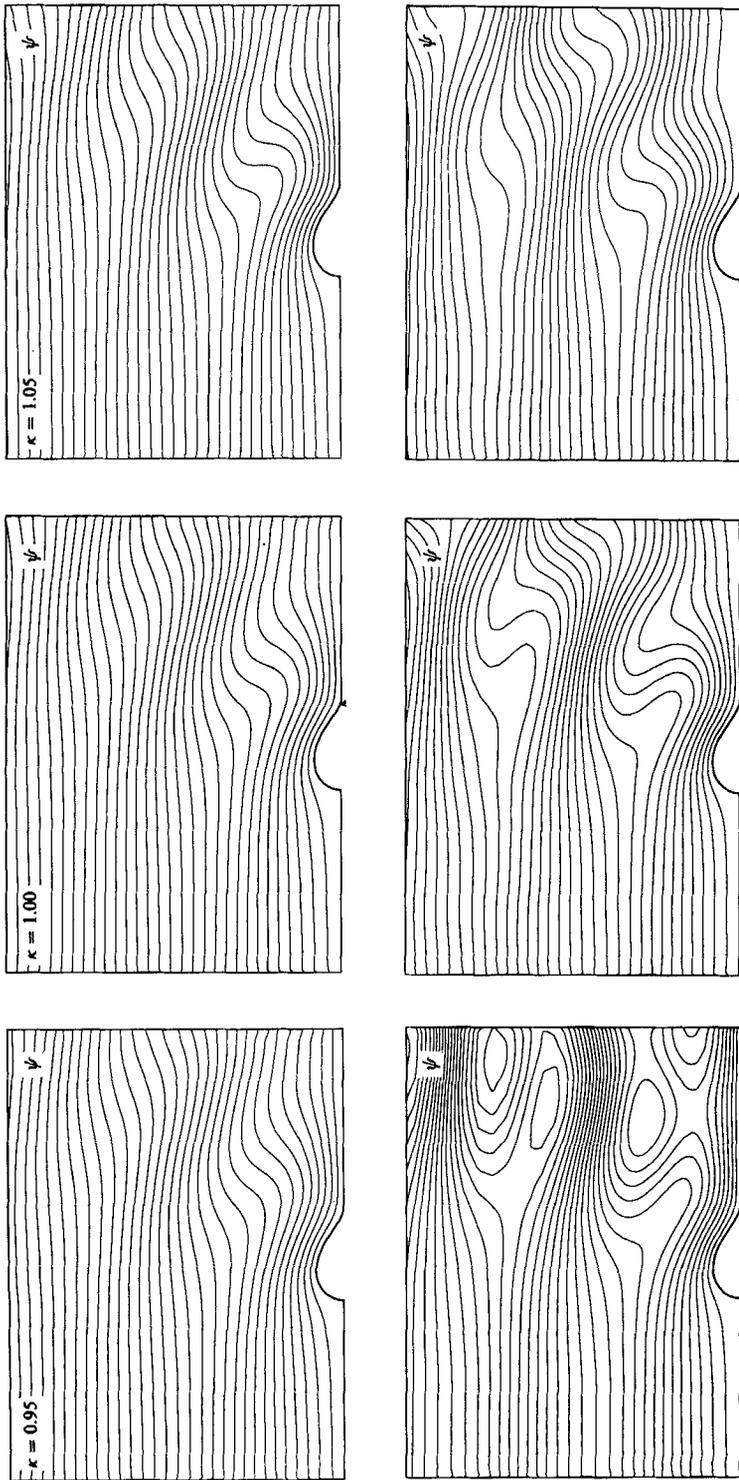
FIGURE 15. The stream function ψ (with $\Delta\psi = 0.5$) for both the numerical solutions with $\lambda = 16$ (above) and Long's model (below) when (a) $\kappa = 0.95$, (b) $\kappa = 1.00$ and (c) $\kappa = 1.05$.

hypothesis that upstream-influence is present in the numerical results. Furthermore, the numerical results during the evolution of the flow show finite-amplitude waves originating in the neighbourhood of the obstacle and propagating upstream and it appears that these waves are able to alter the velocity profile on the approach to the obstacle in such a way as to prevent the closed-streamline regions which would otherwise be present when κW is close to an integer multiple of π. The absence of such regions in the numerical results in figure 15 is unlikely to be solely due to the effect of the Ekman suction term in (2.10) since that dissipation is weak over lengthscales of the order of the obstacle width when λ is large.

11. $E^{\frac{1}{4}}$-layer separation

The parameter regime studied in this paper is such that no effects due to horizontal viscous diffusion are included in the leading-order flow. However, as for non-rotating fluid flow at a high Reynolds number, these effects will always be important in thin boundary-layer regions adjacent to no-slip surfaces. For f-plane flows the effects of these regions, known as $E^{\frac{1}{4}}$ layers, have been studied widely and many of the conclusions reached in those studies (see, for example, Page (1987) for a review) can be immediately extended to the β-plane flow considered here; this is because the governing equations for the layers are, to leading-order, identical for both flows, with the only dependence on α being through the imposed velocity at the outer edge of the layer.

Provided these layers remain thin and attached to the obstacle surface, without separating in the manner shown in Page (1987, 1988), the effect of these layers on the overall flow features can be neglected and the numerical results presented in this paper accurately describe the flow patterns expected in the corresponding experiments. For small values of λ this will almost always be true and the flow features described in §3 will be unaffected by the $E^{\frac{1}{4}}$ layers. However, as seen in Page (1982, 1987), once λ exceeds a certain finite critical value λ_c, which depends on α, it can be shown that the $E^{\frac{1}{4}}$ layers can separate from the obstacle, and the separated shear layers enclose an independent region of flow, bounded by a single value of ψ. Once this has occurred the effective obstacle shape can be extended to include the separated flow region and, as pointed out in §1, the resulting shape for many forms of bluff bodies is then very similar to that of a Joukowski aerofoil. Therefore, the qualitative features of a viscous flow past a bluff obstacle can be expected to be similar to those examined for the inviscid flow past an aerofoil in this paper, although the effective length of the aerofoil would increase with λ for the viscous flow, as the length of the separation bubble expands.

Notwithstanding the above, it is interesting to examine whether the viscous flows corresponding to those calculated in this paper will contain separated $E^{\frac{1}{4}}$ layers. To this end, the necessary condition for separation to occur, used in Page (1982), was examined to determine the range of values of α and λ for which it is satisfied. This requires that the tangential velocity u_0 against the obstacle satisfies the condition

$$\lambda \frac{\mathrm{d}u_0}{\mathrm{d}s} \leqslant -1 \tag{11.1}$$

at some streamwise distance s along the surface, and for each value of α this identifies a lower bound on the value of λ for which separation can occur. The resulting curve has been plotted on figure 9 and is identified by a broken line. Of particular interest is the apparent suppression of separation for small values of α. For larger values of

α this trend reverses and the curve appears to be approaching the $\lambda = 0$ axis, consistent with the analysis in §4, for $\alpha \gg 1$ and $\lambda = O(1/\alpha)$, which suggests that the critical value of λ is probably proportional to $1/\alpha$ in this region, up until the point when α is of order $E^{-\frac{1}{4}}$.

Another point concerning the separation of the $E^{\frac{1}{4}}$ layers is the relevance to this paper of the results of Merkine (1980), Matsuura (1986) and Matsuura & Yamagata (1986), all of which indicate that separation is 'delayed' as the β-effect (i.e. α) is increased. In each of those cases the authors are referring more to the position of the separation point on the obstacle than to whether separation occurs at all (some are effectively considering the case $\lambda = \infty$ for which separation must occur). It is important to distinguish between these two separate meanings of 'delayed separation', particularly when examining the results of §5 of Foster (1985) for which, incidentally, separation will be expected very close to the rear stagnation point once $\bar{\lambda} > \frac{1}{4}$.

Finally, flows in which $E^{\frac{1}{4}}$ layers have separated from the obstacle are likely to become unsteady for sufficiently small values of E, owing to shear-layer instability, and the resulting motion is asymmetric, in the form of a Kármán vortex street. The development of this instability in the context of a driven flow within a cylindrical container has been examined by Becker & Page (1990), where it was found that the separated flow does remain steady over a wide range of parameters.

12. Conclusions

The aim of this study was to examine the phenomenon of upstream influence in a simple, but realistic, situation for which a number of disjoint theoretical results are available, and to combine these with both some new theory and the results of numerical calculations. By doing this a more complete picture of an important geophysical flow has been established, revealing properties which can be generalized both to other β-plane flows and to other configurations displaying upstream-influence effects. Much of this has been achieved through the simplifying effect introduced by the linear friction term (due to Ekman suction in this case), which reduces the influence of the choice of boundary conditions on both the analytical and numerical results. The parameter range studied is that which is also appropriate to the laboratory experiments of Boyer & Davies (1982).

The main conclusion of this work is that most of the flow features identified in each of the asymptotic regimes are present, at least in a modified form, in the flow for $O(1)$ values of α and λ. Of particular note are the downstream 'lee-wavetrain' and the upstream 'blocked' region; in the former case similar features were observed in previous studies using Long's model, for example Miles & Huppert (1968), although the neglect of the upstream-influence effect does appear to overemphasize the amplitude of the steady lee-wavefield in some cases. With regard to the upstream influence, which is introduced (for a finite-width channel) once the ratio α/λ exceeds a critical value, it has been confirmed that the steady upstream waves can have a significant effect on the overall flow field, particularly near resonance, and that for sufficiently large values of α/λ the different wavelength components can combine to form a region of retarded, or 'blocked', flow ahead of the obstacle. The flow considered by Foster (1985) is an extreme case of this general effect. Despite this, the conservation of potential vorticity does yield an order of magnitude estimate for the strength of the lee waves for $\lambda \geqslant O(1/\alpha)$. The separation between those stationary modes which appear upstream of the obstacle and those which appear downstream

can be determined through a group velocity argument and this is unaffected by the presence of Ekman dissipation. In fact, this dissipation simply acts to confine the downstream waves within an $O(\lambda)$ distance of the obstacle, and introduces a maximum upstream decay scale of $(\alpha W^2/\pi^2 - \lambda)$ when that quantity is positive (and L otherwise).

Another important feature, present for large values of α, is the intensification of the flow velocities on the downstream surface of the obstacle, the 'western boundary current'. Numerical calculations suggest that this layer extends into the wake behind the obstacle as inertial effects increase, eventually becoming less noticeable as the layer becomes dominated by nonlinear effects and the lee-wave pattern forms in the wake.

The numerical calculations presented in this study have been obtained by integrating the problem from an initially irrotational state towards a steady state, ensured through the frictional effects of Ekman suction. In a wave-adjustment problem of this kind it is not immediately clear that flow field in the final steady state is not dependent upon the particular initial conditions chosen. As a result, it is quite probable that Long's model (which requires a uniform upstream profile) does yield, in the absence of dissipation, the appropriate solution for the steady state of a particular problem where the upstream waves in the initial condition are exactly annihilated by the upstream-travelling Rossby waves which lead to the eventual steady state. This has not, however, been pursued here. More generally, there does not appear to be any clear correspondence between the initial upstream profile and that which remains once the steady state is attained, so the appropriate function $\mathscr{F}$ for any problem can probably be found only by solving the complete unsteady problem.

In this study the obstacle is considered to have the form of a Joukowski aerofoil, whereas Foster (1985), Matsuura & Yamagata (1986), Miles & Huppert (1968) (in the context of Long's model) and Boyer & Davies (1982) used a circular cylinder. Comparison of both the lee-wave patterns for Long's model solutions and the results of the numerical integrations for different shaped obstacles show that the qualitative features of the flow field are not greatly affected by the choice of obstacle. The most significant difference is in the flow near the trailing edge, particularly in the regimes considered in §4 and §8, where the boundary layers against the body are forced to turn abruptly near the rear stagnation point. This point is pursued in Page & Johnson (1990).

One parameter not examined in this study is the effect of the length L of the obstacle on the flow field. Numerical trails with several values of L indicate that there are no significant qualitative differences in the flow features for each of these and most of the theory outlined in this paper is independent of the value of L, while that value is of $O(1)$. The only noticeable difference is likely to be in the wavenumber distribution of the amplitudes of the various wave components in the steady flow. For $L \gg 1$ the theory in McIntyre (1972), for thin obstacles, can be applied and this suggests that upstream influence becomes less important as L increases, being $O(1/L^2)$ compared to the uniform flow. Furthermore, the critical value for upstream wave-components increases to $\kappa > 2\pi/W$ in that case, since only even values of n, forced by wave-interactions in the lee-wavefield, are found upstream. For long obstacles it can also be expected that some simplifications of the theory are possible since the Laplacian in (6.3) can be replaced by $\partial^2/\partial y^2$, and it is likely that the results in Baines & Guest (1988) for a continuously-stratified flow could be extended, at least partially, to this flow.

Another effect not considered extensively is that due to the finite width $2W$ of the channel, both through its effect on the allowable wavenumbers l in the steady upstream flow and on the introduction of reflected waves into the flow domain. The latter effect was minimized for the values of λ used in this study by choosing a sufficiently large value of W. For a infinite value of W the most significant theoretical differences are that there is no minimum value of α/λ for which steady upstream waves exist and that there is a continuous (rather than discrete) range of allowable wavenumbers l for which these waves exist at any fixed value of α/λ. Since the upstream dissipation scale introduced in §7 is infinite in this limit, it can be expected that the upstream waves decay algebraically (as in, for example, Yamagata 1976), and McIntyre (1972) concludes that upstream disturbances for the internal-gravity-wave case decay algebraically in time. However, it is not expected that these differences would have a significant qualitative effect on the flow fields examined in this paper for most parameter regimes.

REFERENCES

BAINES, P. G. 1977 Upstream influence and Long's model in stratified flows. *J. Fluid Mech.* **82**, 147–159.

BAINES, P. G. & GUEST, F. 1988 The nature of upstream blocking in uniformly stratified flow over long obstacles. *J. Fluid Mech.* **188**, 23–45.

BEARDSLEY, R. C. 1969 A laboratory model of the wind-driven ocean circulation. *J. Fluid Mech.* **38**, 255–271.

BEARDSLEY, R. C. 1973 A numerical investigation of a laboratory analogy of the wind-driven ocean circulation. *Proc. 1972 NAS Symp. on Numerical Methods of Ocean Circulation*, pp. 311–326.

BECKER, A. & PAGE, M. A. 1990 Flow separation and unsteadiness in a rotating sliced cylinder. *Geophys. Astrophys. Fluid Dyn.* (to appear).

BOYER, D. L. & DAVIES, P. A. 1982 Flow past a circular cylinder on a β-plane. *Phil. Trans. R. Soc. Lond.* A **306**, 533–556.

FOSTER, M. R. 1985 Delayed separation in eastward, rotating flow on a β-plane. *J. Fluid Mech.* **155**, 59–75.

GREENSPAN, H. P. 1968 *The Theory of Rotating Fluids*. Cambridge University Press.

GREENSPAN, H. P. 1970 A note on the laboratory simulation of planetary flows. *Stud. Appl. Maths* **48**, 147–152.

GRIMSHAW, R. H. J. & SMYTH, N. 1986 Resonant flow of a stratified fluid over topography. *J. Fluid Mech.* **169**, 429–464.

HENRICI, P. 1974 *Applied and Computational Complex Analysis*, vol. 1. Wiley.

HIDE, R. & HOCKING, L. M. 1979 On detached shear layers and western boundary currents in a rotating homogeneous liquid. *Geophys. Astrophys. Fluid Dyn.* **14**, 19–43.

HUPPERT, H. E. & MILES, J. W. 1969 Lee waves in a stratified flow. Part 3. Semi-elliptical obstacle. *J. Fluid Mech.* **35**, 481–496.

JOHNSON, E. R. 1977 Stratified Taylor columns on a beta plane. *Geophys. Astrophys. Fluid Dyn.* **9**, 159–177.

JOHNSON, E. R. 1978 Quasigeostrophic flow above sloping boundaries. *Deep-Sea Res.* **25**, 1049–1071.

JOHNSON, E. R. & PAGE, M. A. 1990 Flow past a circular cylinder on a β-plane (in preparation).

LIGHTHILL, M. J. 1966 Dynamics of rotating fluids: a survey. *J. Fluid Mech.* **26**, 411–431.

LIGHTHILL, M. J. 1967 On waves generated in dispersive systems by travelling forcing effects, with applications to the dynamics of rotating fluids. *J. Fluid Mech.* **27**, 725–752.

LONG, R. R. 1955 Some aspects of the flow of stratified fluids. III: Continuous density gradients. *Tellus* **7**, 341–357.

McCARTNEY, M. S. 1975 Inertial Taylor columns on a beta plane. *J. Fluid Mech.* **68**, 71–95.

McIntyre, M. E. 1972 On Long's hypothesis of no upstream influence in a uniformly stratified or rotating fluid. *J. Fluid Mech.* **52**, 209–243.

Matsuura, T. 1986 The separation of flow past a circular cylinder on a β-plane. *J. Oceanogr. Soc. Japan* **42**, 362–372.

Matsuura, T. & Yamagata, T. 1986 A numerical study of viscous flow past a right circular cylinder on a β-plane. *Geophys. Astrophys. Fluid Dyn.* **37**, 129–164.

Merkine, L.-O. 1980 Flow separation of a β-plane. *J. Fluid Mech.* **99**, 399–409.

Miles, J. W. 1968 Lee waves in a stratified flow. Part 1. Thin barrier. *J. Fluid Mech,* **32**, 549–567.

Miles, J. W. & Huppert, H. E. 1968 Lee waves in a stratified flow. Part 2. Semi-circular obstacle. *J. Fluid Mech.* **33**, 803–814.

Miles, J. W. & Huppert, H. E. 1969 Lee waves in a stratified flow. Part 4. Perturbation approximations. *J. Fluid Mech.* **35**, 497–525.

Moore, D. W. 1978 Homogeneous fluids in rotation, Section A: Viscous effects. In *Rotating Fluids in Geophysics* (ed. P. H. Roberts & A. Soward). Academic.

Page, M. A. 1982 Flow separation in a rotating annulus with bottom topography. *J. Fluid Mech.* **123**, 303–313.

Page, M. A. 1983 The low Rossby number flow of a rotating fluid past a flat plate. *J. Engng Maths* **17**, 191–202.

Page, M. A. 1987 Separation and free-streamline flows in a rotating fluid at low Rossby number. *J. Fluid Mech.* **179**, 155–177.

Page, M. A. 1988 The numerical calculation of free-streamline flows in a rotating fluid at low Rossby number. In *Computational Fluid Dynamics*, pp. 579–588. North-Holland.

Page, M. A. & Johnson, E. R. 1986 Upstream influence and separation in flow past obstacles on a β-plane. *Proc. 9th Australasian Fluid Mechanics Conference*, pp. 432–435.

Page, M. A. & Johnson, E. R. 1990 Nonlinear western boundary current flow near a corner. *Dyn. Oceans. Atmos.* (submitted).

Pedlosky, J. 1979 *Geophysical Fluid Dynamics.* Springer.

Pedlosky, J. & Greenspan, H. P. 1967 A simple laboratory model for the oceanic circulation. *J. Fluid Mech.* **27**, 291–304.

Stewartson, K. 1958 On the motion of a sphere along the axis of a rotating fluid. *Q. J. Mech. Appl. Maths* **11**, 39–51.

Swarztrauber, P. N. 1974 A direct method for the discrete solution of separable elliptic equations. *SIAM J. Numer. Anal.* **11**, 1136–1150.

Yamagata, T. 1976 A note on boundary layers and wakes in rotating fluids. *J. Oceanogr. Soc. Japan* **32**, 155–161.